iScience

CellPress
OPEN ACCESS

Article

Step-dose IL-7 treatment promotes systemic expansion of T cells and alters immune cell landscape in blood and lymph nodes

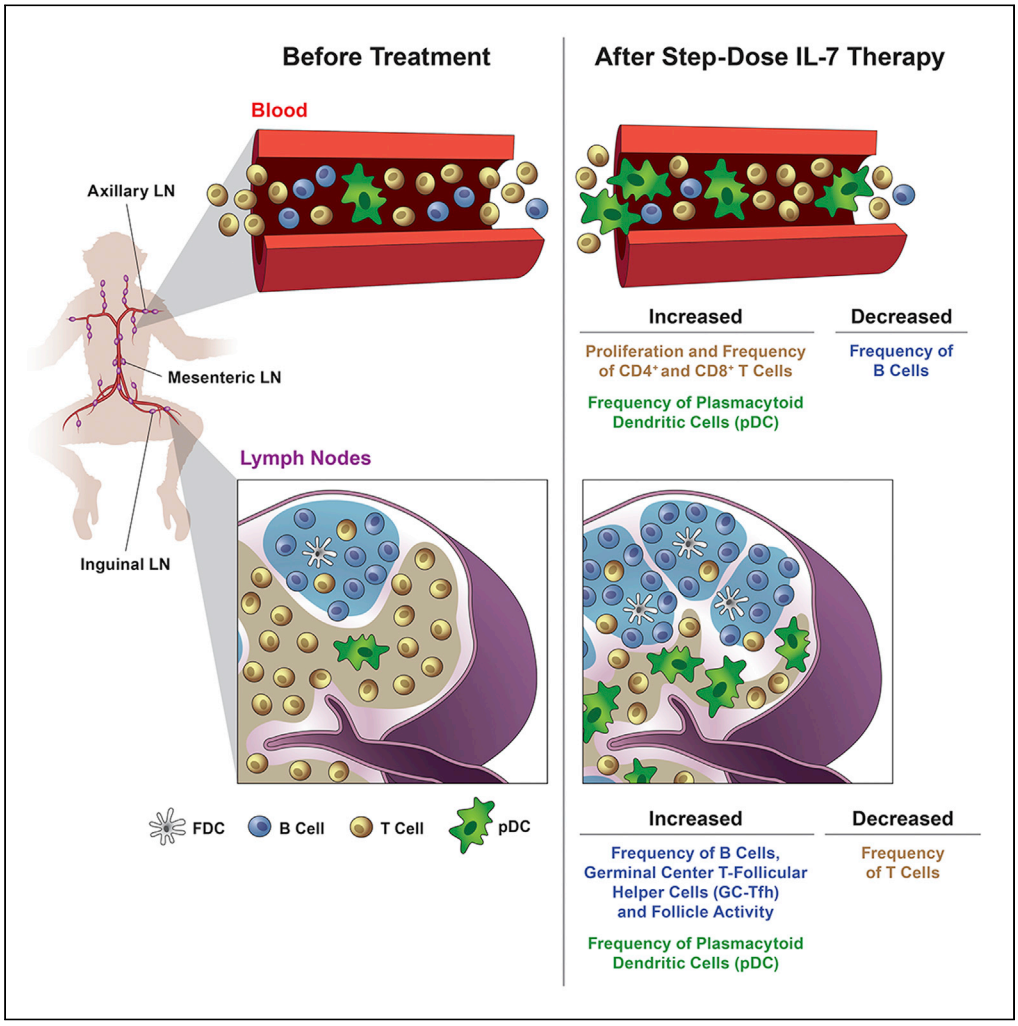

Hrishikesh Pandit, Antonio Valentin, Matthew Angel, ..., Raymond Sowder, Barbara K. Felber, George N. Pavlakis

george.pavlakis@nih.gov

Highlights

Step-dose IL-7 treatment in rhesus macaques induces systemic proliferation of T cells

IL-7 increases pDC frequency, activation, and type-1 interferon signature

Step-dose IL-7 increases germinal center formation and Tfh activity

Pandit et al., iScience 26, 105929
February 17, 2023
https://doi.org/10.1016/j.isci.2023.105929

iScience

CellPress
OPEN ACCESS

Article

Step-dose IL-7 treatment promotes systemic expansion of T cells and alters immune cell landscape in blood and lymph nodes

Hrishikesh Pandit,[1] Antonio Valentin,[1] Matthew Angel,[2,3] Claire Deleage,[4] Cristina Bergamaschi,[5] Jenifer Bear,[5] Raymond Sowder,[4] Barbara K. Felber,[5] and George N. Pavlakis[1,6,*]

SUMMARY

We employed a dose-escalation regimen in rhesus macaques to deliver glycosylated IL-7, a cytokine critical for development and maintenance of T lymphocytes. IL-7 increased proliferation and survival of T cells and triggered several chemokines and cytokines. Induction of CXCL13 in lymph nodes (LNs) led to a remarkable increase of B cells in the LNs, proliferation of germinal center follicular T helper cells and elevated IL-21 levels suggesting an increase in follicle activity. Transcriptomics analysis showed induction of IRF-7 and Flt3L, which was linked to increased frequency of circulating plasmacytoid dendritic cells (pDCs) on IL-7 treatment. These pDCs expressed higher levels of CCR7, homed to LNs, and were associated with upregulation of type-1 interferon gene signature and increased production of IFN-α2a on TLR stimulation. Superior effects and dose-sparing advantage was observed by the step-dose regimen. Thus, IL-7 treatment leads to systemic effects involving both lymphoid and myeloid compartments.

INTRODUCTION

Interleukin 7 (IL-7), a member of the common γ-chain family of cytokines, is a homeostatic cytokine critical for the generation, growth, and survival of T cells, particularly the naive (T_N) and central memory (T_{CM}) subsets. IL-7 binds to the unique alpha chain (CD127/IL-7Rα) of the heterodimeric IL-7 receptor, with signaling mediated by the γ-chain (CD132). This interaction activates the Jak/STAT pathway leading to the phosphorylation of STAT5, translocation of the phosphorylated protein into the nucleus, and activation of genes associated with T lymphocyte growth and survival. IL-7 is mainly produced by mesenchymal, epithelial cells and the lymphatic endothelial cells within lymphoid tissues, including bone marrow, thymus, lymph nodes (LN) and lymphatic vessels. This supports its critical role throughout the entire lymphoid compartment in the control of T cell growth, maintenance of T cell responsiveness and prevention of anergy[1,2]

Adaptive cellular immune responses are generated within secondary lymphoid tissues, where the fibroblastic reticular cells (FRCs) in the T cell zone constitutively produce IL-7 to support survival of IL-7Rα expressing T_N and T_{CM}.[3] IL-7 signaling downregulates IL-7-Rα on terminally differentiated effector T cells, but the receptor is re-expressed after several days and remains expressed during the later contraction phase of the immune response.[4] Moreover, some effector T cells, committed to enter a long-term memory T cell pool, regain expression of IL-7Rα implicating IL-7 as a critical modulator of the effector to memory cell transition.[5,6] In contrast, cells involved in the generation of humoral immune responses such as mature B cells, germinal center follicular T helper (GC-Tfh) and follicular dendritic cells (FDC) do not express IL-7Rα and, therefore, do not respond directly to IL-7.

IL-7 has been used in clinical trials to support immune reconstitution in clinical conditions associated with lymphopenia. The first clinical trial was conducted with non-glycosylated IL-7 (CYT 99 007; Cytheris SA).[7] A glycosylated second-generation IL-7 (CYT107) has also been tested in multiple clinical trials for the treatment of cancer, chronic viral infections (e.g., HIV), sepsis and idiopathic CD4 lymphocytopenia, or for support after hematopoietic stem cell transplantation.[8–17] IL-7 treatment resulted in a dose-dependent expansion of circulating CD4 and CD8 T cells, with increased proliferation and upregulated expression of the anti-apoptotic survival factor Bcl2 in all treated individuals. Because the effects of IL-7 treatment were monitored mainly in blood samples, there is limited information of the systemic effects of IL-7 therapy,

[1]Human Retrovirus Section, Vaccine Branch, Center for Cancer Research, National Cancer Institute at Frederick, Frederick, MD 21702, USA

[2]Vaccine Branch, Center for Cancer Research, National Cancer Institute, Bethesda, MD, USA

[3]Center for Cancer Research Collaborative Bioinformatics Resource, Leidos Biomedical Research, Inc., Frederick National Laboratory for Cancer Research, Frederick, MD 21702, USA

[4]AIDS and Cancer Virus Program, Frederick National Laboratory for Cancer Research, Leidos Biomedical Research, Inc., Frederick, MD 21702, USA

[5]Human Retrovirus Pathogenesis Section, Vaccine Branch, Center for Cancer Research, National Cancer Institute at Frederick, Frederick, MD 21702, USA

[6]Lead contact

*Correspondence: george.pavlakis@nih.gov

https://doi.org/10.1016/j.isci.2023.105929

especially in secondary lymphoid tissues. Complementing the clinical data, several studies in non-human primates[18–25] have demonstrated that IL-7 administration induced T cell proliferation and survival in both peripheral blood and lymph nodes (LNs). The macaque model and clinical trials used a fixed-dose strategy with concentrations varying between 10–200 μg/kg and different time intervals between IL-7 injections.

We have previously shown that administration of heterodimeric IL-15 (hetIL-15), another homeostatic cytokine of the gamma-chain family, in a step-dose escalation protocol, optimizes the bioactivity of hetIL-15 by providing increasing amount of free cytokine to the gradually expanding pool of proliferating target cells in rhesus macaques.[26,27] The rationale for step-dosing was to gradually increase the cytokine levels sufficient to allow step-by-step expansion of responsive lymphocytes and result in a larger number of free receptors on the surface of newly expanded cells. This would then allow optimal usage of increased cytokine concentrations provided in subsequent injections. This approach led to a gradual increase in the pool of target cells optimizing the use of hetIL-15 and eliminating the side effects associated with free cytokine. We hypothesized that using IL-7 in a step-dose regimen would enhance the cytokine pharmacodynamics, improving the therapeutic benefit in lymphopenic conditions or immunological dysregulation associated with several infections, while minimizing toxicity. With this aim, we performed a dose-escalation treatment in rhesus macaques using mammalian cell produced macaque IL-7 in three steps. The IL-7 effects were monitored in peripheral blood and lymphoid tissues, including lymph nodes from several anatomical sites and spleen. We found that IL-7 treatment triggered expression of an array of cytokines/chemokines leading to the redistribution of activated lymphocytes and myeloid cells. Of interest, IL-7 treatment led to increased B cell and Tfh activity within the LN, and expansion of pDCs producing type-1 interferon.

RESULTS

Pharmacokinetics and pharmacodynamics of step-dose IL-7 treatment

The recombinant rhesus macaque IL-7 used in this study was produced and purified from HEK293H cells (Figure S1). Although IL-7 migrated as a 30 kDa molecule in denaturing gels (Figures S1A and S1C), we also observed formation of high molecular weight multimers as shown in native gels (Figures S1B and S1D). The macaque IL-7 was selected to avoid immunogenicity and the potential impairment of biological activity associated with multiple injections. Six rhesus macaques were treated with IL-7 following a dose-escalation protocol. The treatment comprised the delivery of doubling concentrations (50, 100, 200 μg/kg) of IL-7 by subcutaneous injection on days 1, 4 and 8 (Figure 1A). Thisstep-dose escalation protocol was intended to optimize the cytokine consumption by gradually expanding the pool of target cells that require and efficiently bind the increasing amount of free cytokine, as previously described for hetIL-15.[26]

IL-7 plasma levels were analyzed at different time points during treatment. Before treatment, IL-7 plasma concentrations were below the detection limit of the assay (<7.8 pg/mL) in all animals except 15P052. We observed a dose-dependent increase in IL-7 plasma levels at 4 h after each injection (Figure 1B, left panel). The IL-7 trough levels at 48 h also increased after each dose suggesting that the dose escalation regimen extended the availability of free cytokine (Figure 1B, right panel). Using flow cytometry to monitor IL-7Rα (CD127) density on IL-7 treatment, we found significantly lower CD127 surface levels in T cells from LNs collected from different anatomical sites after step-dose IL-7 treatment. These data indicated that IL-7 distribution throughout the lymphatic tissues and suggested substantial occupancy of the cellular binding sites by the injected cytokine (Figure S2).

The treatment was well-tolerated in all animals, with no apparent toxicity or abnormalities in blood chemistry except for transient increases in the aminotransferases and creatine kinase levels (Table S1). Evaluation of complete blood counts (CBC) before and after IL-7 treatment revealed no significant changes in absolute neutrophil, lymphocyte, or platelet counts; a significant decline in circulating monocytes; and an increase in basophil and eosinophil counts in the animals at the end of the IL-7 treatment (Figures S3A–S3F). In addition, red blood cells (RBC) counts were significantly reduced while reticulocyte counts were increased, which suggested an increase in bone marrow activity on IL-7 treatment (Figures S3G and S3H).

Changes in leukocyte populations induced by IL-7 were also monitored by multi-parametric flow cytometry in blood and lymph node (LN) samples collected at different time points during the treatment. We observed an increase in the frequency of cycling ($Ki67^+$) naive and memory $CD4^+$ and $CD8^+$T cells in circulation, with the highest proliferation rate among cells with a central memory (CM) phenotype ($CD95^{hi}CD28^{hi}$) (Figures 1C and S4A). Higher level of proliferation was found within the $CD8^+$T cell subsets

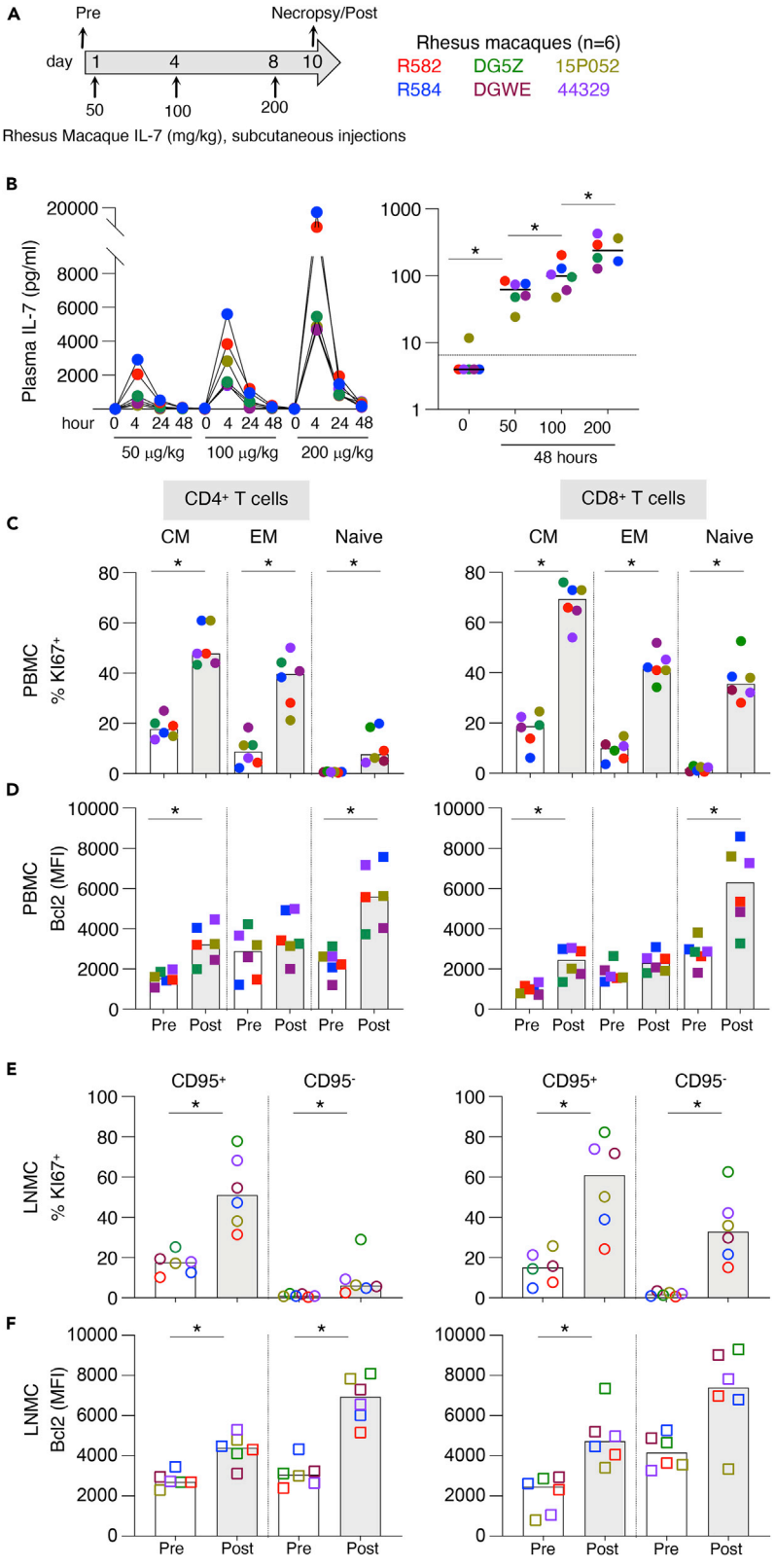
A
Pre
Necropsy/Post
day
1
4
8
10
50
100
200
Rhesus macaques (n=6)
R582
DG5Z
15P052
R584
DGWE
44329
Rhesus Macaque IL-7 (mg/kg), subcutaneous injections
B
Plasma IL-7 (pg/ml)
hour
0 4 24 48 0 4 24 48 0 4 24 48
50 µg/kg
100 µg/kg
200 µg/kg
48 hours
CD4+ T cells
CD8+ T cells
C
CM
EM
Naive
PBMC
% KI67+
D
PBMC
Bcl2 (MFI)
Pre
Post
E
CD95+
CD95-
LNMC
% KI67+
F
LNMC
Bcl2 (MFI)

Figure 1. Pharmacokinetics and pharmacodynamics of IL-7 on step-dose treatment in rhesus macaques

(A) Schematic representation of the IL-7 step-dose treatment. Six rhesus macaques received by subcutaneous injection three doses of increasing amounts of IL-7 administered every three days. The animals were sacrificed two days after the last injection.

(B) IL-7 plasma levels were determined by ELISA in samples collected at the indicated time points after each injection (left panel). IL-7 trough plasma levels were measured 48 h after each injection (days 3, 6 and 10) (right panel). Data from individual animals are shown using the same color-code throughout all the figures.

(C–F) Analysis of T cells in peripheral blood mononuclear cells (PBMC; (C and D)) and lymph node mononuclear cells (LNMC; (E and F)), collected before (pre) and after (post/necropsy) the IL-7 treatment. (C) Percentage of proliferating ($Ki67^+$) and (D) expression of the survival factor Bcl-2 among the CM, EM and naive $CD4^+$ (left panel) and $CD8^+$ (right panel) T cells. Frequency of $Ki67^+$ (E) and expression of Bcl2 (F) in memory and naive $CD4^+$ (left panels) and $CD8^+$ (right panels) T cells from LNMC. Values from individual animals and median are plotted. Asterisk indicates $p < 0.05$, Wilcoxon non-parametric paired t test.

compared to $CD4^+$ subsets (Figure 1C), corresponding to the higher CD127 (IL-7Rα) levels in $CD8^+$ subsets than $CD4^+$ subsets (Figure S4B). Moreover, the naive ($CD95^-CD28^+$) and CM ($CD95^{hi}CD28^{hi}$) T cells expressed similar levels of the IL-7R and showed a significant increase in their proliferation activity after IL-7 treatment (Figure S4). Although only a subset of naive T cells was cycling (~10% and ~30% for CD4 and CD8, respectively) at the end of the treatment (Figure 1C), the dominant response of naive T cells to the IL-7 treatment was characterized by an increase in the anti-apoptotic factor Bcl2 (Figure 1D). A less pronounced increase in Bcl2 was also observed in $CD4^+$ and $CD8^+$T cell with CM phenotype, but it was absent in the EM ($CD95^+CD28^-$) subset (Figure 1D).

T cell changes in secondary lymphoid tissues upon IL-7 treatment

IL-7-induced T cell changes were monitored in secondary lymphoid tissues collected at necropsy from several anatomical locations. $CD4^+$ and $CD8^+$ T lymphocytes from different LNs (axillary, inguinal, mediastinal, and mesenteric) as well as spleen showed a significant increase in proliferation rate, as assessed by Ki67 expression, after IL-7 treatment compared to similar samples from untreated control animals (Figures S5A and S5B, respectively). We observed similar levels of proliferation across different anatomical sites. Like in PBMC, the proliferative responses induced by IL-7 in secondary lymphoid tissues were higher among the $CD8^+$ than the $CD4^+$T cell subsets.

CD95 expression was used to distinguish between memory ($CD95^+$) and naive T cells ($CD95^-$) within the LN. More than 90% of $CD95^+$T cells exhibited a phenotype of CM, with EM T cells representing only a minor population within the LN. Direct comparison of the pre-treatment LN sample (collected from each animal before starting IL-7 treatment) with LN collected at necropsy revealed that IL-7 triggered more robust proliferative responses in the memory T cell subsets compared to the naive population (Figure 1E). Like in the PBMCs, the naive T cell response to the IL-7 treatment was characterized by higher survival signal (Bcl2 expression) than in the memory T cells (except macaque 15P052 in $CD8^+$T cells) (Figure 1F) and by an increase of memory T cells and a relative decrease in the percentage of naive T cells (Figures S5C and S5D). This trend was similar for both $CD4^+$ and $CD8^+$T cells, however, this change reached statistical significance only for $CD4^+$ in our animal cohort. Taken together, these data indicate that the step-dose IL-7 treatment leads to increased levels of circulating cytokine with systemic proliferation and higher Bcl2 levels, indicating improved survival of T cells in both blood and secondary lymphoid compartments.

IL-7 treatment triggers several biological pathways in PBMC and LNMC

To further dissect the effect of IL-7 treatment, we performed gene expression analysis on PBMC and LNMC samples before and after cytokine administration, using a panel of 776 NHP specific barcoded probes, covering 18 immune-related signaling pathways (NanoString Technology). The mRNA transcripts identified by the probes were quantitated and subjected to pathway analysis. A total of 173 genes were differentially regulated in the PBMC samples of which 74 were upregulated and 99 were downregulated. In LNMC, 226 genes were differentially regulated; 96 were upregulated and 130 were downregulated after IL-7 treatment (Figures 2A and 2B, Tables S2 and S3). Analysis of the data using Gene Ontology (GO) database revealed that the differentially regulated genes belonged to several immunological pathways. IL-7 treatment led to an upregulation of a set of genes belonging to the negative regulation of apoptotic signaling pathway (GO:2001234 - PBMC $p = 0.01$; LNMC $p = 0.0003$) both in PBMCs and LNMCs. In agreement with increased survival (Bcl2) described in Figure 1, we found increased *Bcl-2* gene expression in our transcriptomic analysis. In addition, a common upregulated pathway in both PBMC and LNMC was defense

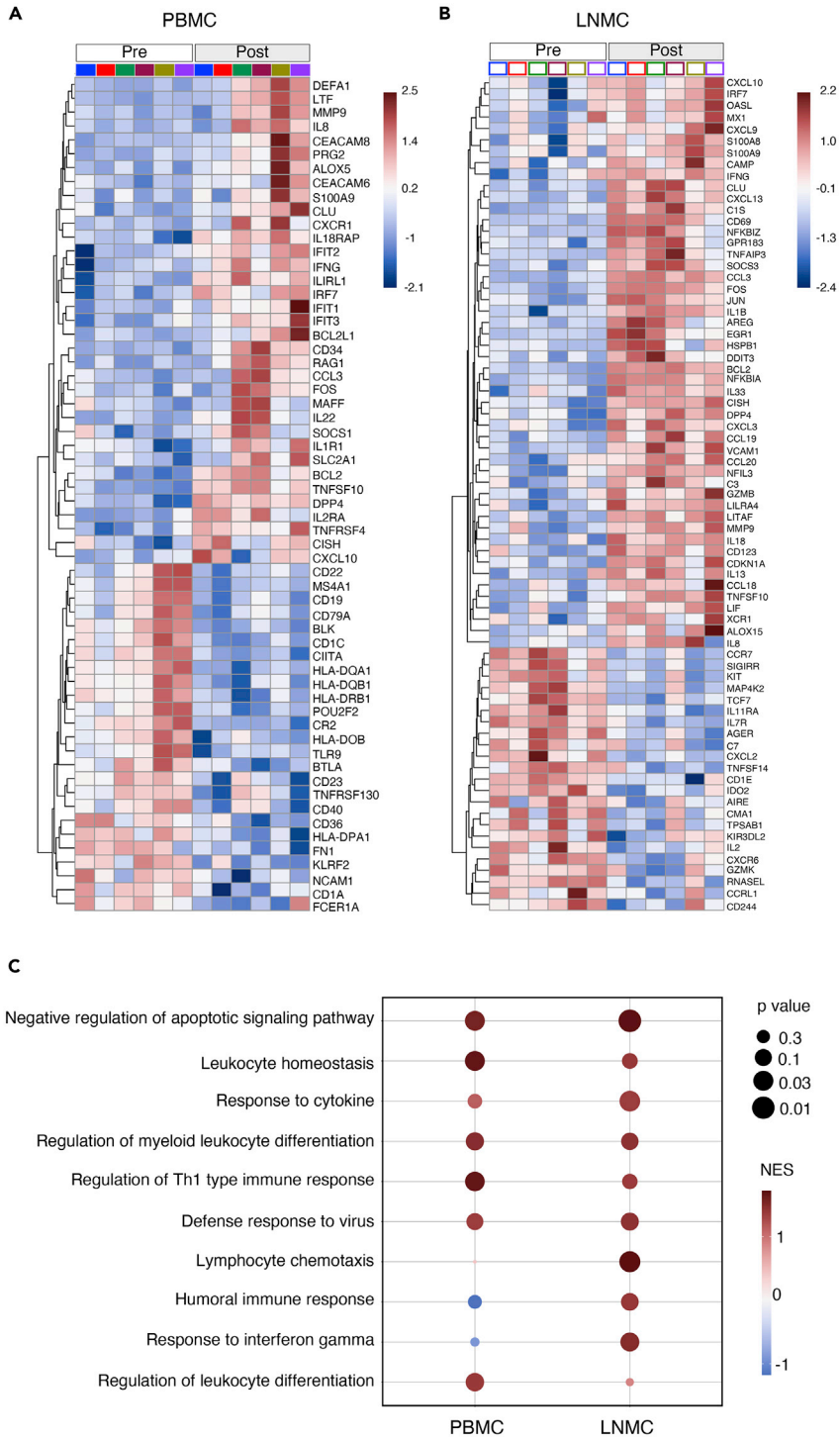

Figure 2. Transcriptomics analysis of PBMCs and LNMCs

Heat maps depicting differentially regulated genes in (A) PBMC and (B) LNMC samples before and after IL-7 treatment. (C) Pathway analysis of the transcriptomics data using Gene Ontogeny (GO) database. Several pathways were significantly affected in both PBMC and LNMC whereas some were exclusively altered in either sample.

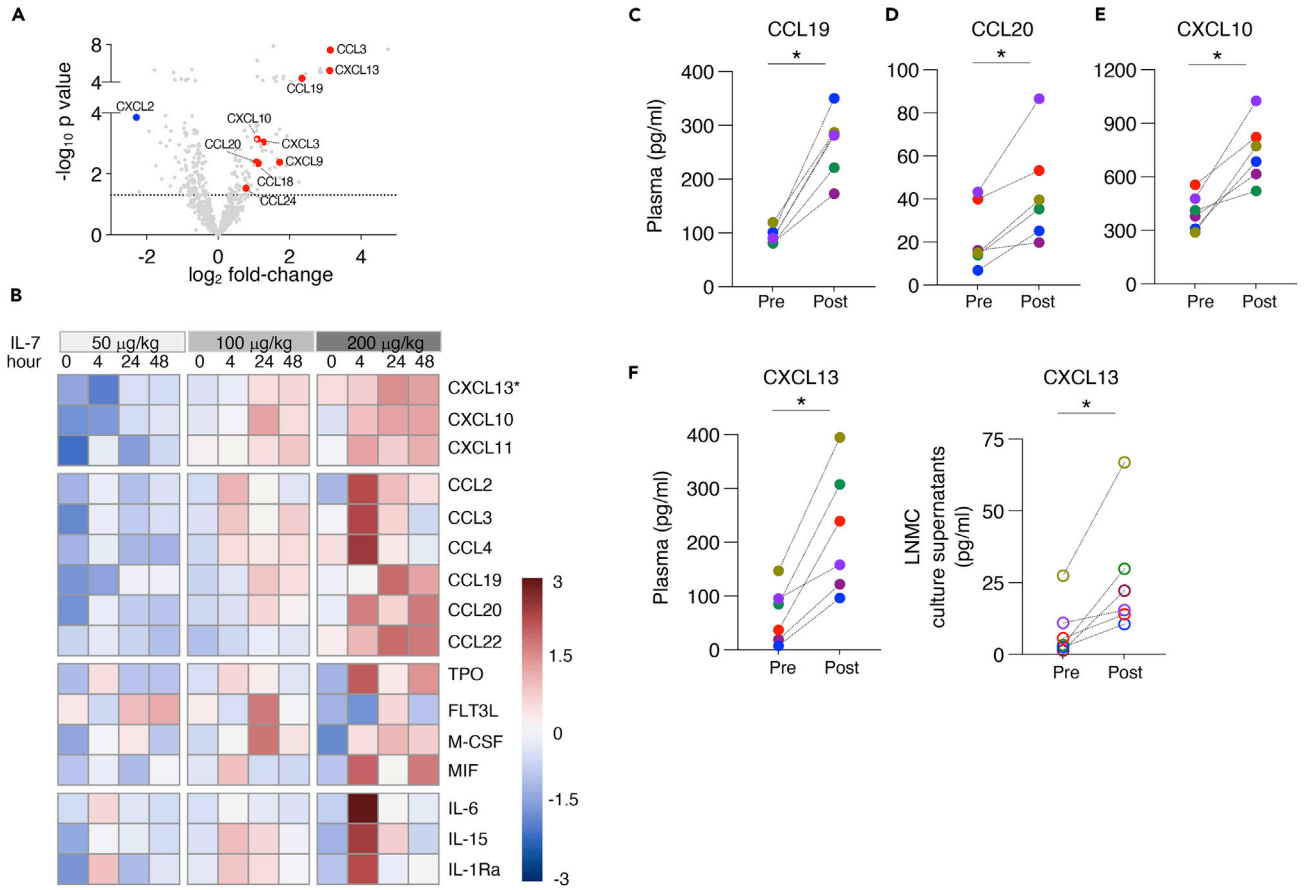

Figure 3. Plasma chemokines after IL-7 treatment

(A) Volcano plot depicting differentially expressed genes in LN. Log2 fold change (L2FC) (red line) and $p < 0.05$ (p value for multiple comparison; blue line) are indicated. Red dots indicate significantly upregulate transcripts.

(B) Heatmap showing average plasma values of all six animals for each analyte and timepoint with changes after IL-7 treatment. Plasma samples collected at 4, 24 and 48 h after each IL-7 injection were analyzed by a chemiluminescent assay (Meso Scale Diagnostics, 61 plex) and ELISA (for CXCL13).

(C–F) Levels of chemokines before and after IL-7 treatment depicting (C) CCL19, (D) CCL20, (E) CXCL10 in plasma, and (F) CXCL13 in plasma (left panel) and spontaneously released *ex vivo* by LNMC (right panel). Values from individual animals are shown. Asterisk denotes $p < 0.05$, Wilcoxon non-parametric paired t-test.

response to virus (GO:0051607 - PBMC p = 0.06; LNMC p = 0.04) which includes IFN-α regulated genes such as IRF7, CXCL10, IFNG, MX2, NLRP3, CXCL9, OASL, IFIT2, MX1, IFIT1 and regulation of myeloid leukocyte differentiation (GO:0002761 - PBMC p = 0.03; LNMC p = 0.05) (Figure 2C). Of interest, lymphocyte chemotaxis (GO:0048247 - LNMC p = 0.009) and humoral immune response (GO:0006959 - LNMC p = 0.04) pathways were significantly upregulated only in LNMCs (Figure 2C). The transcriptomics data suggested that systemic delivery of IL-7 triggered direct and indirect effects on lymphocytes and the myeloid cell compartment, with impact on immune cell proliferation, trafficking, and potentially survival.

Step-dose IL-7 treatment stimulates the production of multiple chemokines

Lymphocyte chemotaxis was one of the upregulated pathways in the LN after IL-7 treatment. In LN, RNA transcripts for the chemokines CCL3, CCL19, CCL20, CXCL10 and CXCL13 were significantly upregulated (Figure 3A), suggesting increased recruitment within the LN of CCR5, CCR7, CCR6, CXCR3 and CXCR5 expressing cells. To confirm these findings, we measured cytokine/chemokine changes in plasma using an electro chemiluminescent multiarray assay (MSD) capable of measuring 61 different analytes (Table S4) and we also measured CXCL13 by ELISA. Several analytes including interleukins, growth factors and chemokines showed changes in plasma levels after IL-7 treatment (Figure 3B). A dose-dependent peak in the plasma concentration of several C-X-C and C-C chemokines, i.e., CXCL13, CXCL10 (IP-10), CXCL11 (iTAC), CCL2 (MCP-1), CCL3 (MIP-1a), CCL4 (MIP-1b), CCL19 (MIP-3b), CCL20 (MIP-3a), CCL22, TPO, M-CSF, MIF,

IL-6, IL-15 and IL-1Ra was observed either at 4 or 24 h after each injection. Two days after the last injection, plasma levels of CCL19 (Figure 3C), CCL20 (Figure 3D), CXCL10 (Figure 3E) and CXCL13 (Figure 3F, left panel) were still significantly elevated, consistent with the transcriptomic data. Also, in agreement with the transcriptomic analysis, mononuclear cells from LN collected on IL-7 treatment spontaneously produced significantly higher levels of CXCL13 *ex vivo* than cells from LN obtained before the IL-7 treatment (Figure 3F, right panel). Overall, these data demonstrate that systemic IL-7 delivery induced a robust chemokine(s) response within lymph nodes. This prompted us to analyze changes in different immune cell subset in blood and lymph nodes after IL-7 treatment.

Changes in the frequency of B cells in blood and LNs after step-dose IL-7 treatment

CXCL13 is the chemokine responsible for recruiting $CXCR5^+$ cells, mainly B lymphocytes and $CD4^+$ T follicular helper (Tfh) cells within the follicle in LNs. Induction of a strong CXCL13 gradient within LN led us to monitor the changes in the frequency of B cells. Mature B lymphocytes, either in the circulation or resident in LN, do not express the IL-7R, therefore, do not respond directly to the cytokine treatment. Before IL-7 treatment, the frequency of B cells within the LN ranged from 21%–38% of total LNMCs, but this frequency was significantly increased, to 58%–64%, after the treatment (Figure 4A, left panel). This increase in the relative frequency of B cells led to a concomitant proportional decrease in T cells resulting in a significantly augmented B:T cell ratio in LN (Figure 4A, right panel). We did not observe any increase in the rate of B cell proliferation or Bcl-2 expression on IL-7 treatment (Figure S6), suggesting the most likely mechanism responsible for the increased B cell population within the LN was migration from the periphery. In support of this mechanism, we observed a reduction in the relative frequency of circulating B cells in the blood after IL-7 treatment with an increase in the relative frequency of T cells (Figure 4B, left panel) leading to lower B:T cell ratio in the blood (Figure 4B, right panel).

The B cell population in the LNs was also analyzed by immunohistochemistry (IHC). Staining of LN sections with anti-CD20 antibody revealed increased number of B cell follicles after IL-7 treatment (Figure 4C). In addition, Bcl6 staining revealed a greater number of germinal center (GC)-rich follicles in the LNs after IL-7 treatment in 4 of the 5 animals analyzed (Figures 4D and 4E).

Taken together, IL-7 treatment triggered a CXCL13 gradient promoting B cells infiltration from the periphery into the lymph nodes, and the formation of follicles with increased germinal center activity.

IL-7 treatment affects follicular helper T (Tfh) cells activity within the LN

The increase in CXCL13 levels and the subsequent recruitment of B lymphocytes within LNs prompted us to investigate whether $CXCR5^+$T cells, especially follicular helper T (Tfh) cells, may also be affected by the IL-7 treatment. Based on the expression of PD-1, we divided the LN $CD4^+$ $CXCR5^+$T cells into $CXCR5^+$ $PD\text{-}1^{neg}$, $CXCR5^+$ $PD\text{-}1^+$ (Tfh) and $CXCR5^{hi}$ $PD\text{-}1^{hi}$ germinal center Tfh (GC-Tfh) (Figure S7A) and compared their frequency and proliferative responses on IL-7 treatment (Figure 5A). Of interest, expression of PD-1 inversely correlated with the levels of CD127 (IL-7Ra) within the LN $CXCR5^+$ $CD4^+$T cells, showing the lowest CD127 levels among the fully differentiated GC-Tfh cells (Figure S7B). This analysis showed no differences in the frequency of $CD4^+CXCR5^+PD\text{-}1^{neg}$ and Tfh after IL-7 treatment (Figures S7C and S7D, left panels), whereas the frequency of GC-Tfh was increased in 4 of 6 animals (Figure 5B, left panel), despite their low or no expression of CD127. Of interest, all the $CXCR5^+CD4^+$ subsets, including the Tfh and GC Tfh (characterized by low or no CD127 expression) had a significantly increased proliferation rate (Figure 5B, right panel; Figures S7C and S7D, right panels). These data suggested that IL-7 triggered such effects on GC-Tfh via an indirect mechanism.

Immunofluorescence staining combining antibodies targeting CD4, BCL6 and Ki67 also revealed an increased frequency of proliferating $CD4^+$T cells within the germinal center on IL-7 treatment (Figure 5C, left panel). In agreement with the data obtained by flow cytometry, all macaques analyzed showed significantly increased GC-Tfh proliferation on IL-7 treatment (Figure 5C, right panel).

Tfh activation is linked to IL-21 production, a key cytokine for germinal center formation and Tfh differentiation.[28] We monitored IL-21 plasma levels and found a significant increase of the cytokine in the experimental macaques (except in macaque 15P052) after IL-7 treatment, possibly a reflection of the increased Tfh activity (Figure 5D). The increase in the GC-rich B cell follicles together with GC-Tfh cell proliferation suggested enhanced follicular activity. This may be the result of changes in the expression of genes

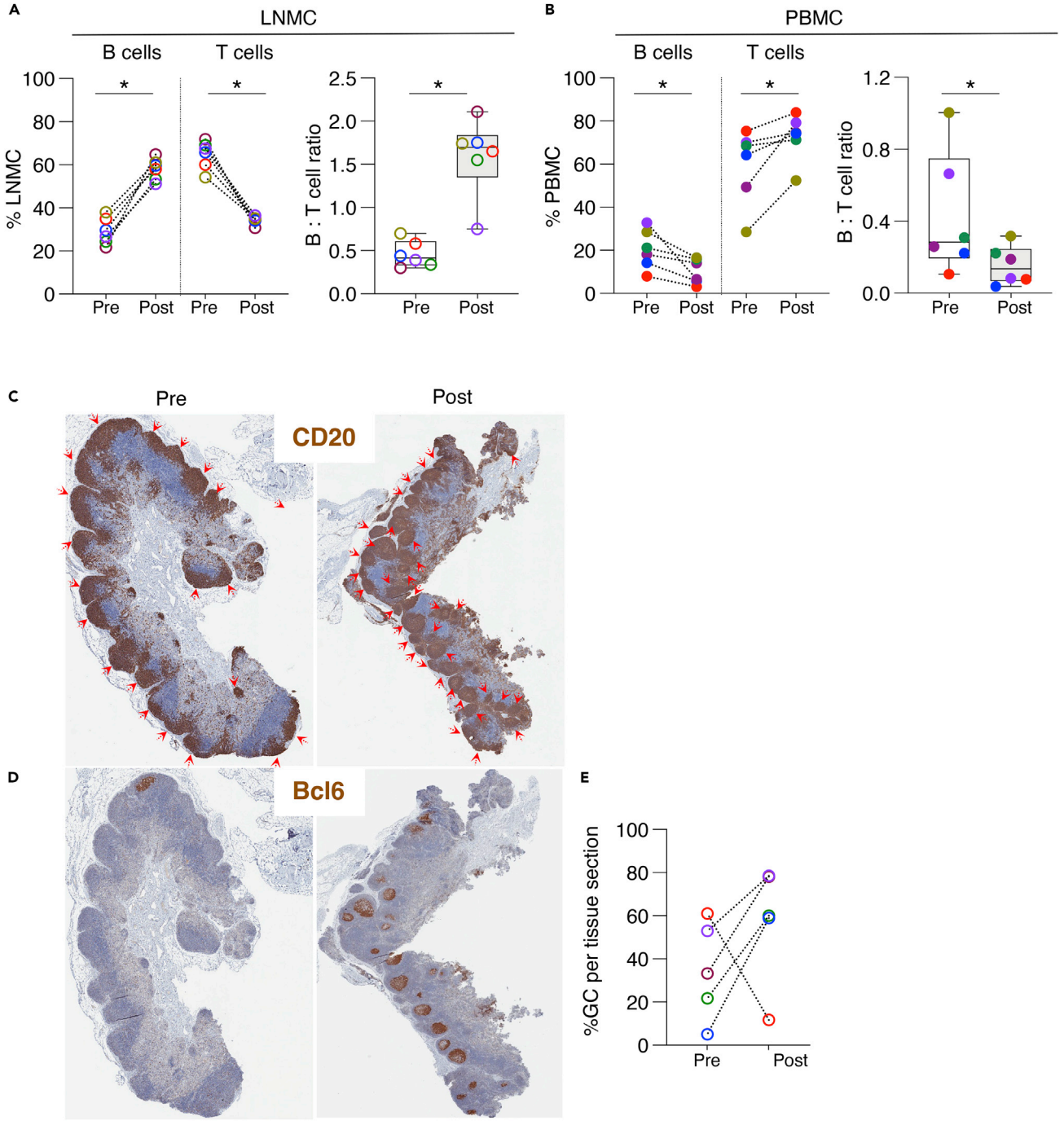

Figure 4. Lymphocyte changes in lymph node and blood on IL-7 treatment

(A) Frequency of T ($CD3^+$) and B ($CD20^+$) lymphocytes (left panel) and changes in the (B):T cell ratio (right panel) within (A) LNMC and (B) PBMC. Asterisk indicates $p < 0.05$, Wilcoxon non-parametric paired t-test.

(C and D) Analysis of B cell follicles and germinal center (GC) within LN tissue sections with immune-histochemistry staining using CD20 and BCL6 antibodies. Representative image (animal R582) of the whole lymph node sections of (C) CD20 and (D) BCL6 staining detected with DAB (brown) and color stained with hematoxylin (blue) before (left panels) and after (middle panels) IL-7 treatment.

(E) Quantification of the percentage of germinal center-positive follicles as % of total number of B cell follicles per tissue section (n = 5) in LN collected before and after IL-7 treatment.

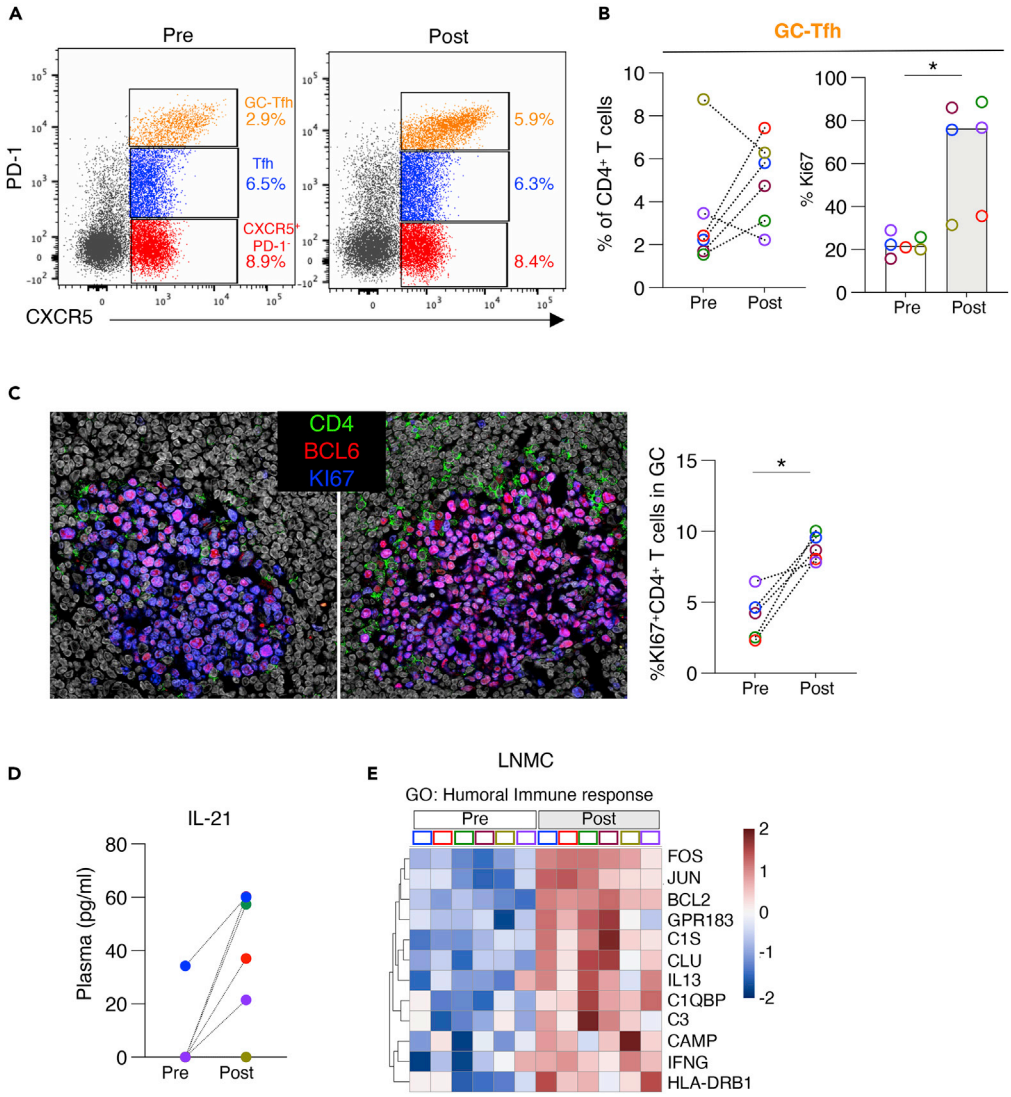

Figure 5. Changes in Tfh cells on IL-7 treatment

(A) Representative dot plots (animal R584) showing the changes in the frequency of CXCR5^{hi}PD-1^{hi} (GC-Tfh).

(B) Analysis of changes in CD4^{+}T cells with frequency of GC-Tfh (left panel) and proliferating (Ki67^{+}) GC-Tfh (right panel).

(C) Immunofluorescence staining targeting CD4, BCL6 and Ki67 *in situ*. Representative pictures of CD4 (green), BCL6 (red) and Ki67 (blue) with DAPI (gray) in sections of lymph nodes taken before and after IL-7 treatment (left panel). Quantification of the percentage of Tfh cells expressing Ki67 within germinal centers (Fiji software) (right panel). Asterisk indicates $p < 0.05$, Wilcoxon non-parametric paired t test.

(D) Levels of IL-21 measured by ELISA in plasma samples.

(E) Heatmap showing changes in the expression of genes associated with humoral response (based on annotation by GO database).

functionally linked to the development of humoral immune responses after IL-7 treatment. In support of this hypothesis, transcriptomic analysis of LNMCs showed that the humoral immune response pathway (GO:0006959, $p = 0.047$) was significantly upregulated and mRNA transcripts of genes such as *FOS, JUN, C1S, CLU, IL-13, C1QB, C3, IFNG, HLA-DRB1* in this pathway were increased in all six animals (Figure 5E).

IL-7 affects the plasmacytoid dendritic cells

Among the pathways affected by IL-7 treatment, regulation of myeloid leukocyte differentiation (GO:0002761 - PBMC $p = 0.03$; LNMC $p = 0.05$) was enriched (Figure 2C) in PBMC and LNMC. In PBMC,

transcripts of genes such as *FLT3-L, TNFSF10 (TRAIL), IFNG* and Interferon Regulatory Factor 7 (*IRF7*) belonging to this pathway were increased (Figure 6A). IRF7 is a critical transcription factor for the activation of type I interferon genes, a hallmark of plasmacytoid dendritic cells (pDCs), which are the main producers of IFN-α. Moreover, FLT3-L is a key growth factor that binds to FLT3 (CD135), a receptor expressed mainly by multipotent progenitor cells and is critical in the development of pDCs. Corroborating the increase in mRNA, we observed an increase in the levels of FLT3-L at 24 h after each IL-7 injection in the plasma of all the treated animals (Figure 6B). Based on these data, we evaluated changes in the frequency of pDCs on IL-7 treatment. pDCs were identified as lineage marker negative ($CD3^-$, $CD20^-$, $CD14^-$, $CD11c^-$) cells expressing MHC-II, $CD123^+$ (IL-3R) and $CD4^+$ (Figure S8A). Flow cytometric analysis of PBMC using this gating strategy demonstrated a significant increase in the frequency of circulating pDCs in all animals (Figure 6C, left panel). This increase reached up to 5-fold in some animals as compared to blood samples collected before IL-7 treatment (Figure 6C, right panel). These circulating pDCs also expressed higher levels of CCR7 at the end of the treatment (Figure 6D), suggesting enhanced capability to migrate toward the LNs in response to the increased CCL19 gradient described above (Figures 3A and 3B). Similar flow cytometric analysis performed on LNMC demonstrated a remarkable increase in the frequency of pDCs after IL-7 treatment (Figure 6E, left panel). The change in pDCs on IL-7 treatment in LN ranged from 5 to 33-fold, was clearly more pronounced than in PBMC (Figure 6E, right panel). This increase in pDC frequency was also observed in spleens as compared to historical frozen spleen samples from untreated control macaques (Figure S8B).

pDCs express high levels of TLR7 and TLR9, two innate immune receptors that recognize pattern motifs. TLR7 and TLR9 detect ssRNA and unmethylated CpG DNA sequences, respectively, and this recognition leads to production of IFN-α by pDCs. To ascertain the functional relevance of the increased frequency of pDCs in lymph nodes, LNMC, collected before and after IL-7 treatment, were treated with the TLR ligands resiquimod (R848) and CpG-C ODN (ODN) *ex vivo*, two compounds that stimulate the production, via TLR-7 and TLR-9 respectively, of IFN-α2a by pDCs.[29,30] Measurements of IFN-α2a in the supernatants at 24 h after stimulation showed that four animals increased the production of IFN-α2a in response to both TLR ligands, whereas the remaining two animals, interestingly, responded to either ODN or R848 (Figure 6F). One explanation of this observation could be differential levels of TLR7 or TLR9 in the pDCs in these two animals, a feature that could not be addressed in this study.

Taken together, IL-7 treatment led to substantial increase in pDC frequency in the LN and enhanced IFN-α2a production in response to TLR-stimulation. Transcriptomic analysis of LNMC showed an enrichment of pathway related to defense response to virus (GO:0051607; $p = 0.04$). Genes belonging to this pathway reflect an IFN-α signature and include genes like IRF-7, the transcription factor highly expressed by pDCs and IFN-α regulated genes such as *MX1, MX2, OASL, IFI44, IFIT1, IFIT2, IFNG, CXCL9* and *CXCL10* (Figure 6G).

Our data demonstrated that step-dose IL-7 treatment increased the pDC population in PBMC and further increased their levels in the LNs. These changes, together with the changes on B and T cell populations, may significantly affect the generation of adaptive immune responses in secondary lymphoid organs.

Fixed-dose IL-7 regimen

The success of the step-dose protocol raised the question of its comparison to a fixed-dose administration of IL-7, as used in previous studies. We treated four macaques with a fixed-dose regimen of either 200 μg/kg (2 animals) or 100 μg/kg (2 animals) IL-7 following an identical three injections protocol as the step-dose (Figure 7A). Total cytokine delivered was 600 μg/kg or 170% and 300 μg/kg or 86% of the step-dose for the animals receiving 200 μg/kg and 100 μg/kg respectively. Samples were analyzed following the same schedule, and using the same methods as the step-dose treated macaques. IL-7 plasma levels peaked at 4 h after each injection in the animals treated with the fixed-dose (Figure 7B). The trough levels at 24 h and 48h after each fixed-dose injection were similar (Figure 7C) and contrasting with the increased trough levels found on the step-dose protocol (Figure 7D), indicating lower bioavailability of free IL-7 in the plasma using the fixed-dose protocol.

We observed a comparable effect in the proliferative responses of $CD4^+$ and $CD8^+$T cells (as determined by Ki67) in IL-7 fixed-dose protocol both in blood and lymph nodes (Figures S9A and S9B) as in step-dose

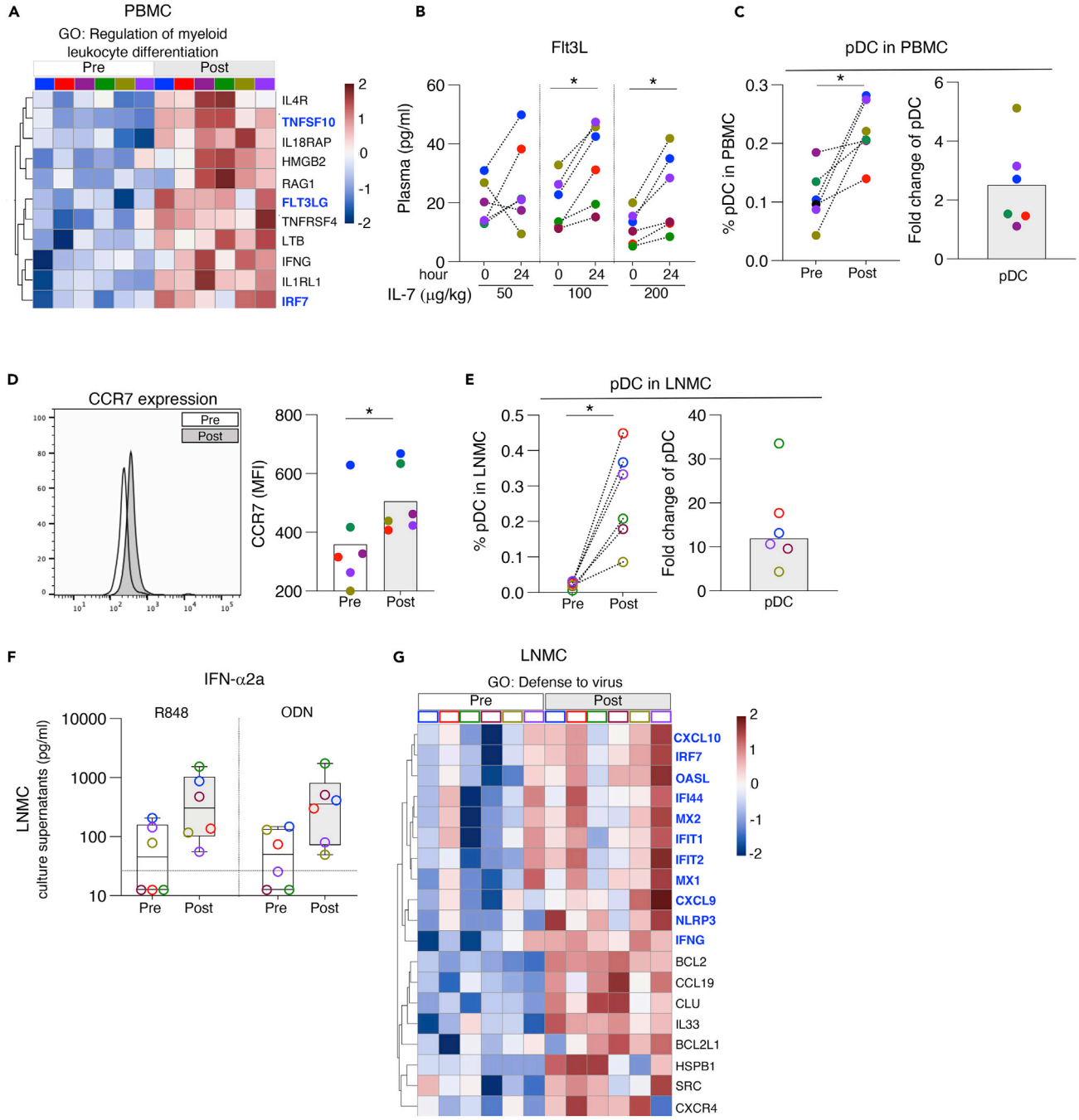

Figure 6. Increase in pDC activity in PBMC and LNMC on IL-7 treatment

(A) Heatmap showing changes of differentially expressed genes associated with the regulation of myeloid leukocyte differentiation pathway in PBMC (based on GO database).

(B) Levels of FLT-3L, measured by the MSD assay, in plasma at 24 h after each IL-7 injection.

(C) Changes in the frequency of pDC in total PBMC (left panel) and fold-change (ratio) is plotted (right panel).

(D) Histogram overlay showing CCR7 expression on pDC from one representative animal (animal R582) before (black line) and after (gray area) IL-7 treatment (left panel). CCR7 (MFI) on pDC is shown (right panel).

(E) Frequency of pDC in total LNMC (left panel) and fold change is plotted (right panel).

(F) Production of IFN-α2a by LNMC treated with R848 and ODN *ex vivo*. The dotted line indicates the detection threshold.

(G) Heatmap showing changes of differentially expressed genes from the response to virus pathway (based on GO database) in the LNMC samples. Genes annotated in blue font belong to the type-1 interferon response. Asterisk in different panels denotes $p < 0.05$, Wilcoxon non-parametric paired t test.

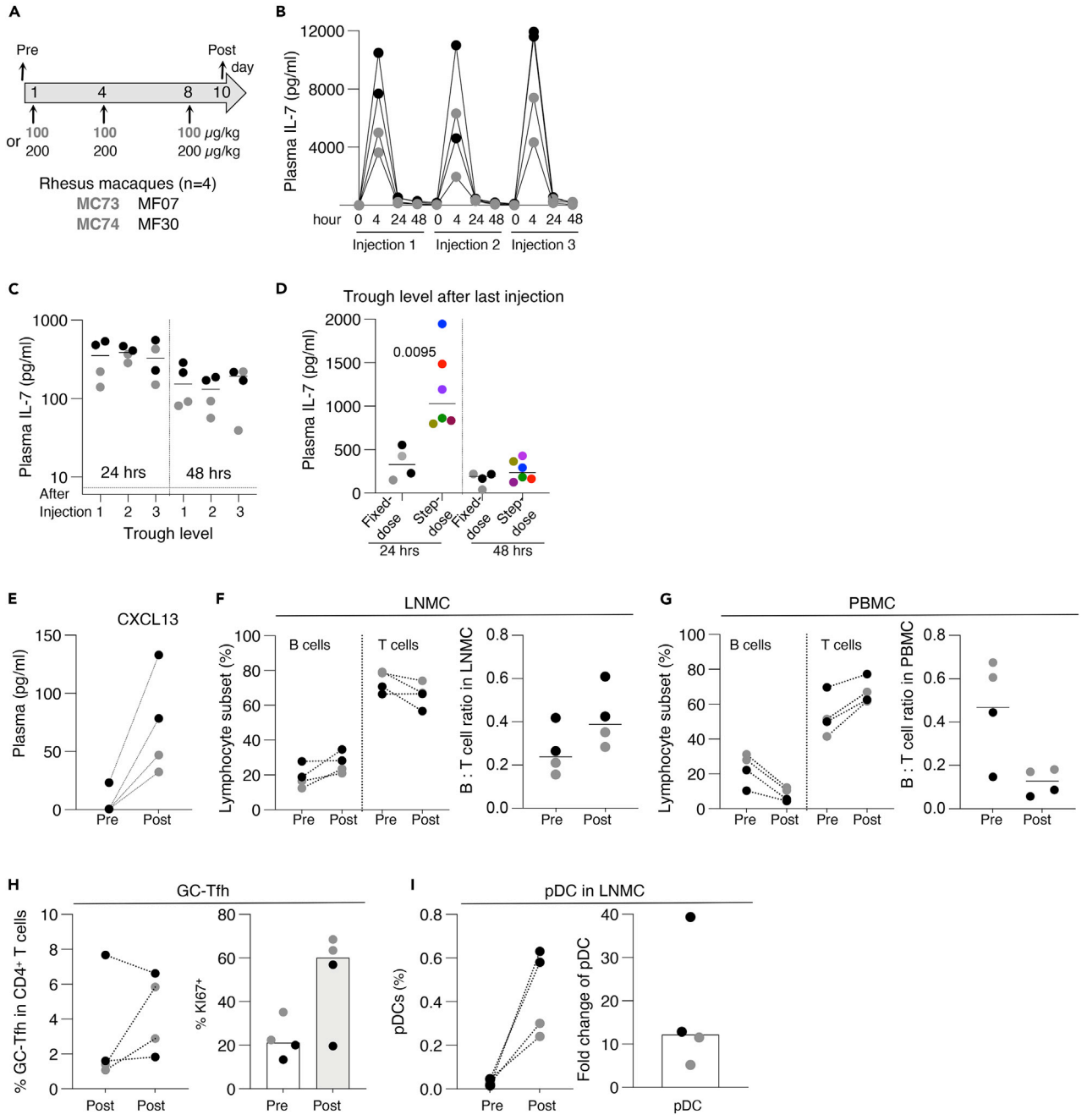

Figure 7. Effects of fixed dose IL-7 treatment

(A) Schematic representation of the IL-7 fixed-dose protocol. Four macaques received subcutaneous injection of three doses of 100 mg/kg (MC73, MC74; gray symbols) or 200 mg/kg (MF07, MF30; black symbols) of IL-7 administered every three days.

(B) Plasma IL-7 levels collected at the indicated time points after each injection.

(C) IL-7 trough levels in plasma were measured 24 h and 48 h after each injection.

(D) Comparison of plasma IL-7 levels at 24 h and 48 h after last cytokine injections in the fixed-dose and step-dose regimen.

(E) CXCL13 levels in plasma before (pre) and after last (post) fixed-dose treatment.

(F) Frequency of B ($CD20^+$) and T ($CD3^+$) lymphocytes in LNMC at pre and post (2 days after last injection) (left panel). B to T cell ratio in LNMC at pre and post (right panel).

(G) Frequency of B ($CD20^+$) and T ($CD3^+$) lymphocytes in PBMC at pre and post (2 days after last injection) (left panel). B to T cell ratio in PBMC at pre and post (right panel).

Figure 7. *Continued*
(H) Changes of frequency of GC-Tfh within CD4$^+$T cells (left panel) and frequency of proliferating (Ki67$^+$) GC-Tfh (CXCR5hi PD-1hi) (right panel).
(I) Frequency of pDC in total LNMC (left panel) and fold change (right panel).

(Figure 1C) treated animals. The fixed-dose protocol led to lower (~2.7x fold) induction of CXCL13 in plasma (Figure 7E) as compared to the step-dose. As a result, the fixed-dose treatment resulted in a modest increase in the frequency of B cells in the LNs (Figure 7F) compared to the step-dose (Figure 4A), leaving T lymphocytes as the dominant population after IL-7 treatment. The change in the frequency of GC-Tfh was also less prominent on fixed-dose treatment (2/4 animals; Figure 7H) compared to step-dose treatment (4/6 animals; Figure 5B).

Plasma levels of Flt3L (Figure S9C) were increased, and an increase of pDCs was found in LN, with stronger response in the 200 μg/kg dose treated animals (Figure 7I). Although similar qualitative responses were observed in the two regimens, the step-dose protocol induced a more robust proliferation of T cells (direct targets) and increase in the frequency of B cells, GC-Tfh and pDCs (indirect targets), altering the immune cell landscape. In addition, the step-dose regimen also provided a dose-sparing effect. We observed equivalent or superior responses with a step-dose protocol using 58% of the total cytokine (350 μg/kg versus 600 μg/kg) of the fixed dose.

DISCUSSION

In this study, we evaluated a step-dose regimen in rhesus macaques to identify effects of IL-7 throughout the body. The treatment stimulated systemic proliferation and survival of T cells, and triggered redistribution of several leukocyte populations. An important effect was the migration of B lymphocytes within lymph nodes, following changes in several chemokine gradients. In addition, IL-7 increased the frequency of pDCs and induced a type-1 interferon gene signature in blood and secondary lymphoid organs. These findings suggest that IL-7 treatment established an immune cell landscape in the LN that may favor stronger adaptive humoral immune responses, a property that supports the use of IL-7 as a vaccine enhancer in prophylactic and therapeutic settings requiring potent antibody responses.

Effectiveness of IL-7 therapy in reconstituting the T cell pool is well-established. Pre-clinical NHP models[18,19,21–25] and clinical trials implemented a fixed-dose regimen with varying time intervals between doses [reviewed in[1]]. A fixed-dose regimen of cytokine administration may not be optimal for achieving maximal pharmacological effects with minimal toxicity. We took advantage of our previous experience implementing a dose-escalation protocol for *in vivo* delivery of hetIL-15. Like IL-7, hetIL-15 is a homeostatic cytokine that promotes the growth and survival of several leukocyte subsets.[26,27] The rationale for implementing a step-dose protocol for IL-7 was that the lower levels of exogenous IL-7 will induce proliferation of target cells resulting in their gradual expansion from the steady-state. Subsequently, the increasing doses of IL-7 would maximize cytokine usage and minimize potential toxicity or off-target effects of free cytokine. Our IL-7 step-dose protocol was found to be safe, well-tolerated and able to stimulate systemic changes that have not been previously reported. We evaluated the effects of step-dose IL-7 treatment in secondary lymphoid organs from different anatomical sites and found that IL-7 stimulates CD4$^+$ and CD8$^+$T cell proliferation in all LNs as well as in spleen, demonstrating that the IL-7 delivered subcutaneously resulted in biodistribution throughout the body.

Several studies have reported rapid induction of IL-7 in tissues during acute phase of viral and bacterial infections.[31–35] Increased IL-7 expression was reported in small intestine of SIV-infected rhesus macaques with transcripts of several chemokines.[36,37] We observed a rapid increase in the plasma concentration of several chemokines, including CCL2, CCL3 and CCL4 after IL-7 injection, a finding previously described in macaques.[36,37] Our transcriptomic analysis identified LNs as the source of several chemokines including CCL3, CCL18, CCL19, CCL24, CXCL10 and CXCL13. This suggested that step-dose IL-7 treatment may directly affect the redistribution of several cell types such as T and B lymphocytes and myeloid cells expressing various chemokine receptors. The CCL19-CCR7 axis directs LN homing of CCR7 expressing lymphocytes and antigen-presenting cells (APCs). It is possible that changes in the cellular composition within lymphoid tissue are the result of two independent mechanisms: (i) cell entry into the LNs following a chemokine gradient (CCL19), and (ii) IL-7-induced local proliferation of T cells.

Lymphoid organ formation depends on the combined effects of IL-7, CCL19 and CXCL13.[38–41] During lymph node development, IL-7 produced by stromal organizer cells,[42] promotes the survival of the IL-7R^{+} lymphoid tissue inducer (LTi) cells,[43] which initiate formation of the LN environment.[44] It has been shown that IL-7 determines the size of the LTi cell pool in adults.[45] Moreover, IL-7 transgenic mice accumulate LTi cells that initiate formation of ectopic lymphoid tissue.[46] It is possible that IL-7 administration stimulates LTi cells in the LNs that may trigger CCL19 and CXCL3 to recruit T and B cells, respectively. In our study, the CXCL13-CXCR5 axis was also affected on IL-7 treatment. CXCL13, a chemokine linked to germinal center activity[47] that mediates entry of CXCR5^{+} B cells and Tfh into the follicles, was significantly increased after IL-7 treatment. The increased CXCL13 production established a chemokine gradient that attracted B lymphocytes toward the LN and shifted the B:T cell ratio. The lower B cell frequency in peripheral blood together with the increased non-proliferating B cell population in the LN on IL-7 treatment suggest that B lymphocytes enter the LN from the periphery following a CXCL13 gradient.

In addition to increased B cells in the LN, IL-7 treatment stimulated the proliferation and activation of GC-Tfh, a cell population characterized by the lack of CD127 expression. Although the reason for the increased Tfh proliferation remains unknown, IL-21 plasma levels were significantly elevated on IL-7 treatment. IL-21 is a hallmark of Tfh activation and is essential to sustain the germinal center reaction[48,49] and Ig class-switching.[50–52]In murine models, provision of IL-7 has been shown to enhance B cell activity and antibody production during influenza infection or on vaccination against rabies.[53,54] Similarly, mucosal delivery of IL-7 was shown to promote leukocyte infiltration and modulate local antibody production on mucosal delivery of a diphtheria toxin vaccine.[55] Moreover, Zhang et al.[56] showed that IL-7 with IL-2 enhanced the immunogenicity of a DNA vaccine by increasing antibody titers, T cell proliferation and IFN-γ production. Our data suggest that IL-7 impacts several key steps in the development and activation of B cell responses within the follicle, potentially leading to a multi-pronged activity that drives a robust antibody response.

Analysis of systemic effects on step-dose IL-7 treatment revealed some additional insights. We found Flt3L upregulation at both mRNA and protein levels. Flt3L is crucial for the production, expansion, and mobilization of DC subsets, particularly pDCs.[57,58] It was reported that administration of CDX-301, a recombinant Flt3L analog, resulted in peripheral expansion of pDCs in humans.[59] Similarly, in our study, IL-7-dependent upregulation of Flt3L led to expansion of pDCs in blood and LN. pDCs are antigen-presenting cells and the major source of type-1 interferon *in vivo*. pDCs differentiate in the bone marrow from a common lymphoid progenitor (CLP) that express CD127 and CD135, the receptor for Flt3L; therefore IL-7 is essential for the production and differentiation of pDCs.[60] We noted that pDCs express higher levels of CCR7 after IL-7 treatment, enabling their entry into the LN following the CCL19 gradient. The increased frequency of pDCs in LN after IL-7 treatment was also associated with a type-I IFN gene signature and increased IFN-α production on TLR stimulation. IRF-7, the master regulator of type-I interferon, and several interferon-stimulated genes (ISGs)[61,62] were also increased on IL-7 treatment. The functional relevance of the IL-7 effects on pDCs was suggested in a mouse model, where intranasal administration of Fc-fused IL-7 resulted in protection against lethal influenza infection, and this protection correlated with increased frequency of pDCs within the lungs.[63] The changes we observed on IL-7 treatment suggested that IL-7 modulates the immune cell landscape in the LN and may favor a stronger humoral response, an activity that could be employed in protocols that incorporate the use of IL-7 as a vaccine enhancer.

Taken together, the results indicate that IL-7 therapy acts at different levels in the immune system. T cell immunity could be strengthened by promoting redistribution, survival, and proliferation of T cells, whereas the influx of B cells and Tfh activation can result in improved humoral immune responses. The role of IL-7 at the interface of cell and humoral adaptive immunity can be exploited in vaccine strategies. Because IL-7 functions at the apex of lymphopoiesis in the bone marrow and is crucial for lymph node development, our findings demonstrate the importance of delineating the systemic effects of IL-7 beyond its direct targets.

We report that the step-dose delivery of IL-7 may have several advantages over the fixed-dose regimen. Although the primary function of supporting proliferation and survival of T cells systemically were comparable in both IL-7 regimens, there was a pronounced increase in homing of B cells and frequency of GC-Tfh

in animals treated bystep-dosing. Intriguingly, the amount of IL-7 required in a dose-escalation protocol was significantly less than required in a fixed-dose regimen. Previously, we have shown that step-dosing of hetIL-15, another homeostatic cytokine like IL-7, results in gradual expansion of cytotoxic cells and has several advantages over fixed-dosing.[26] IL-15 interacts with CD122/CD132 (IL-2Rβ-γ) predominantly on effector CD8 T cells and NK cells whereas IL-7 exerts its function via CD127/CD132 (IL-7Rα-γ) present on naive and central memory T cell subsets. Because the distribution of the respective receptors for these two cytokines is largely non-overlapping, the functional outcomes of the respective step-dose regimens are distinct. The properties of the corresponding receptors may also contribute. For example, the increase in subsequent 48 trough levels of IL-7 (Figure 1B, right panel) could be the result of CD137 downregulation; in contrast, the IL-15 receptor CD122 continues to be expressed in activated lymphocytes. Further study of the differences in the results of step-dose regimens of these two cytokines will provide additional insights on the complex *in vivo* interactions. In summary, we show that a gradual dose-escalation regimen has an overall superior systemic biological effect and should be considered for homeostatic cytokine therapeutic applications.

IL-7 has strong immunotherapeutic potential. Several clinical trials have been conducted using IL-7 to treat lymphocytopenia, and as immune therapeutic agent in cancer, sepsis and infectious diseases.[1] However, our efforts toward developing new delivery protocols and understanding additional IL-7 systemic effects reveal beneficial activities that can be harnessed in different pre-clinical and clinical settings. The study also underscores some similarities of IL-7 action and severe COVID conditions, where both lymphopenia and depletion of pDCs with impaired type I interferon production are the main immunological features that correlate with the severity, predictors of hospitalization and poor prognosis.[64–68] The data presented in this work suggest that step-dose IL-7 treatment could be a useful approach for the treatment of SARS-CoV-2 infected people with severe COVID-19.

In conclusion, IL-7 treatment promoted proliferation of T cells and increase of B lymphocytes in LN together with activated Tfh cells and pDC producing type-1 interferon, an immune landscape that may result in enhanced cellular and humoral adaptive immune responses.

Limitations of the study

A limitation of this work is the small number of animals available for comparison. Although the macaque immune system is very similar to human, the observed effects may differ in humans, especially in magnitude. Additional studies are required for the optimization of IL-7 dosing for different clinical uses.

STAR★METHODS

Detailed methods are provided in the online version of this paper and include the following:

- KEY RESOURCES TABLE
- RESOURCE AVAILABILITY
  - Lead contact
  - Materials availability
  - Data and code availability
- EXPERIMENTAL MODEL AND SUBJECTDETAILS
- METHOD DETAILS
  - Purification of mammalian cell produced rhesus macaque IL-7
  - IL-7 treatment
  - Isolation of PBMCs and preparation of single cell suspensions from LNs and spleen
  - Immune phenotyping and flow cytometry
  - Measurement of plasma cytokines
  - Gene expression analysis by nCounter NHP Immunology Panel
  - Immunohistochemistry for B cells and germinal center count
  - Immuno-histofluorescence for Tfh $Ki67^+$ quantification
  - *Ex vivo* stimulation of lymph node mononuclear cells (LNMC) with TLR ligands
  - Statistics
  - Bioinformatics

- QUANTIFICATION AND STATISTICAL ANALYSIS
  - Software

SUPPLEMENTAL INFORMATION

Supplemental information can be found online at https://doi.org/10.1016/j.isci.2023.105929.

ACKNOWLEDGMENTS

We thank D. Weiss, J. Treece, J. Misamore and staff (BIOQUAL, Inc.) for excellent support with the macaque studies; E. Chertova and J.D. Lifson, Biological Products Core and Retroviral Protein Chemistry Core of the AIDS and Cancer Virus Program, Frederick National Laboratory, for assistance with IL-7 purification; Y. Wang and J. Inglefield, Clinical Services Program, Frederick National Laboratory for Cancer Research; X. Wu and N. Bubunenko, Genomics Laboratory, Frederick National Laboratory for Cancer Research; A. Kane for graphics; M. Rosati for discussions, R. Burns for technical assistance and T. Jones for editorial assistance. This work was supported in part by funding from the Intramural Research Program, National Institutes of Health, National Cancer Institute, Center for Cancer Research to G.N.P. and B.K.F. and with Federal Funds from the National Cancer Institute, National Institutes of Health, under contracts number 75N91019D00024 and HHSN261200800001E to C.D. The content of this publication does not necessarily reflect the views or policies of the Department of Health and Human Services, nor does mention of trade names, commercial products, or organizations imply endorsement by the U.S. Government.

AUTHOR CONTRIBUTIONS

H.P., A.V., B.K.F., and G.N.P. conceptualization. H.P., A.V., G.N.P., and B.K.F. methodology.

H.P., A.V., C.D., J.B., R.S., and M.A. investigation. H.P., M.A., C.D., and B.K.F. visualization.

G.N.P. and B.K.F. provided funding acquisition and project administration. A.V., G.N.P., and B.K.F. supervised the project. H.P. wrote the original draft of the manuscript. H.P., A.V., C.B., B.K.F., and G.N.P. wrote, reviewed, and edited the manuscript. All authors read and approved the final manuscript version.

DECLARATION OF INTERESTS

The authors declare no competing interests.

INCLUSION AND DIVERSITY

We support inclusive, diverse, and equitable conduct of research.

Received: August 2, 2022
Revised: November 6, 2022
Accepted: January 3, 2023
Published: February 17, 2023

REFERENCES

1. Barata, J.T., Durum, S.K., and Seddon, B. (2019). Flip the coin: IL-7 and IL-7R in health and disease. Nat. Immunol. *20*, 1584–1593. https://doi.org/10.1038/s41590-019-0479-x.

2. Mackall, C.L., Fry, T.J., and Gress, R.E. (2011). Harnessing the biology of IL-7 for therapeutic application. Nat. Rev. Immunol. *11*, 330–342. https://doi.org/10.1038/nri2970.

3. Link, A., Vogt, T.K., Favre, S., Britschgi, M.R., Acha-Orbea, H., Hinz, B., Cyster, J.G., and Luther, S.A. (2007). Fibroblastic reticular cells in lymph nodes regulate the homeostasis of naive T cells. Nat. Immunol. *8*, 1255–1265. https://doi.org/10.1038/ni1513.

4. Park, J.H., Yu, Q., Erman, B., Appelbaum, J.S., Montoya-Durango, D., Grimes, H.L., and Singer, A. (2004). Suppression of IL7Ralpha transcription by IL-7 and other prosurvival cytokines: a novel mechanism for maximizing IL-7-dependent T cell survival. Immunity *21*, 289–302. https://doi.org/10.1016/j.immuni.2004.07.016.

5. Rubinstein, M.P., Lind, N.A., Purton, J.F., Filippou, P., Best, J.A., McGhee, P.A., Surh, C.D., and Goldrath, A.W. (2008). IL-7 and IL-15 differentially regulate CD8+ T-cell subsets during contraction of the immune response. Blood *112*, 3704–3712. https://doi.org/10.1182/blood-2008-06-160945.

6. Kaech, S.M., Tan, J.T., Wherry, E.J., Konieczny, B.T., Surh, C.D., and Ahmed, R. (2003). Selective expression of the interleukin 7 receptor identifies effector CD8 T cells that give rise to long-lived memory cells. Nat. Immunol. *4*, 1191–1198. https://doi.org/10.1038/ni1009.

7. Rosenberg, S.A., Sportès, C., Ahmadzadeh, M., Fry, T.J., Ngo, L.T., Schwarz, S.L., Stetler-Stevenson, M., Morton, K.E., Mavroukakis, S.A., Morre, M., et al. (2006). IL-7 administration to humans leads to expansion of CD8+ and CD4+ cells but a relative decrease of CD4+ T-regulatory cells. J. Immunother.

29, 313–319. https://doi.org/10.1097/01.cji.0000210386.55951.c2.

8. Lévy, Y., Sereti, I., Tambussi, G., Routy, J.P., Lelièvre, J.D., Delfraissy, J.F., Molina, J.M., Fischl, M., Goujard, C., Rodriguez, B., et al. (2012). Effects of recombinant human interleukin 7 on T-cell recovery and thymic output in HIV-infected patients receiving antiretroviral therapy: results of a phase I/IIa randomized, placebo-controlled, multicenter study. Clin. Infect. Dis. *55*, 291–300. https://doi.org/10.1093/cid/cis383.

9. Sereti, I., Estes, J.D., Thompson, W.L., Morcock, D.R., Fischl, M.A., Croughs, T., Beq, S., Lafaye de Micheaux, S., Yao, M.D., Ober, A., et al. (2014). Decreases in colonic and systemic inflammation in chronic HIV infection after IL-7 administration. PLoS Pathog. *10*, e1003890. https://doi.org/10.1371/journal.ppat.1003890.

10. Katlama, C., Lambert-Niclot, S., Assoumou, L., Papagno, L., Lecardonnel, F., Zoorob, R., Tambussi, G., Clotet, B., Youle, M., Achenbach, C.J., et al. (2016). Treatment intensification followed by interleukin-7 reactivates HIV without reducing total HIV DNA: a randomized trial. AIDS *30*, 221–230. https://doi.org/10.1097/QAD.0000000000000894.

11. Thiébaut, R., Jarne, A., Routy, J.P., Sereti, I., Fischl, M., Ive, P., Speck, R.F., D'Offizi, G., Casari, S., Commenges, D., et al. (2016). Repeated cycles of recombinant human interleukin 7 in HIV-infected patients with low CD4 T-cell reconstitution on antiretroviral therapy: results of 2 phase II multicenter studies. Clin. Infect. Dis. *62*, 1178–1185. https://doi.org/10.1093/cid/ciw065.

12. Francois, B., Jeannet, R., Daix, T., Walton, A.H., Shotwell, M.S., Unsinger, J., Monneret, G., Rimmelé, T., Blood, T., Morre, M., et al. (2018). Interleukin-7 restores lymphocytes in septic shock: the IRIS-7 randomized clinical trial. JCI Insight *3*, e98960. https://doi.org/10.1172/jci.insight.98960.

13. Sheikh, V., Porter, B.O., DerSimonian, R., Kovacs, S.B., Thompson, W.L., Perez-Diez, A., Freeman, A.F., Roby, G., Mican, J., Pau, A., et al. (2016). Administration of interleukin-7 increases CD4 T cells in idiopathic CD4 lymphocytopenia. Blood *127*, 977–988. https://doi.org/10.1182/blood-2015-05-645077.

14. Pachynski, R.K., Morishima, C., Szmulewitz, R., Harshman, L., Appleman, L., Monk, P., Bitting, R.L., Kucuk, O., Millard, F., Seigne, J.D., et al. (2021). IL-7 expands lymphocyte populations and enhances immune responses to sipuleucel-T in patients with metastatic castration-resistant prostate cancer (mCRPC). J. Immunother. Cancer *9*, e002903. https://doi.org/10.1136/jitc-2021-002903.

15. Perales, M.A., Goldberg, J.D., Yuan, J., Koehne, G., Lechner, L., Papadopoulos, E.B., Young, J.W., Jakubowski, A.A., Zaidi, B., Gallardo, H., et al. (2012). Recombinant human interleukin-7 (CYT107) promotes T-cell recovery after allogeneic stem cell transplantation. Blood *120*, 4882–4891. https://doi.org/10.1182/blood-2012-06-437236.

16. Sportès, C., Babb, R.R., Krumlauf, M.C., Hakim, F.T., Steinberg, S.M., Chow, C.K., Brown, M.R., Fleisher, T.A., Noel, P., Maric, I., et al. (2010). Phase I study of recombinant human interleukin-7 administration in subjects with refractory malignancy. Clin. Cancer Res. *16*, 727–735. https://doi.org/10.1158/1078-0432.CCR-09-1303.

17. Trédan, O., Ménétrier-Caux, C., Ray-Coquard, I., Garin, G., Cropet, C., Verronèse, E., Bachelot, T., Rebattu, P., Heudel, P.E., Cassier, P., et al. (2015). ELYPSE-7: a randomized placebo-controlled phase IIa trial with CYT107 exploring the restoration of CD4+ lymphocyte count in lymphopenic metastatic breast cancer patients. Ann. Oncol. *26*, 1353–1362. https://doi.org/10.1093/annonc/mdv173.

18. Aspinall, R., Pido-Lopez, J., Imami, N., Henson, S.M., Ngom, P.T., Morre, M., Niphuis, H., Remarque, E., Rosenwirth, B., and Heeney, J.L. (2007). Old rhesus macaques treated with interleukin-7 show increased TREC levels and respond well to influenza vaccination. Rejuvenation Res. *10*, 5–17. https://doi.org/10.1089/rej.2006.9098.

19. Beq, S., Nugeyre, M.T., Ho Tsong Fang, R., Gautier, D., Legrand, R., Schmitt, N., Estaquier, J., Barré-Sinoussi, F., Hurtrel, B., Cheynier, R., and Israël, N. (2006). IL-7 induces immunological improvement in SIV-infected rhesus macaques under antiviral therapy. J. Immunol. *176*, 914–922. https://doi.org/10.4049/jimmunol.176.2.914.

20. Fry, T.J., Moniuszko, M., Creekmore, S., Donohue, S.J., Douek, D.C., Giardina, S., Hecht, T.T., Hill, B.J., Komschlies, K., Tomaszewski, J., et al. (2003). IL-7 therapy dramatically alters peripheral T-cell homeostasis in normal and SIV-infected nonhuman primates. Blood *101*, 2294–2299. https://doi.org/10.1182/blood-2002-07-2297.

21. Leone, A., Rohankhedkar, M., Okoye, A., Legasse, A., Axthelm, M.K., Villinger, F., Piatak, M., Jr., Lifson, J.D., Assouline, B., Morre, M., et al. (2010). Increased CD4+ T cell levels during IL-7 administration of antiretroviral therapy-treated simian immunodeficiency virus-positive macaques are not dependent on strong proliferative responses. J. Immunol. *185*, 1650–1659. https://doi.org/10.4049/jimmunol.0902626.

22. Moniuszko, M., Fry, T., Tsai, W.P., Morre, M., Assouline, B., Cortez, P., Lewis, M.G., Cairns, S., Mackall, C., and Franchini, G. (2004). Recombinant interleukin-7 induces proliferation of naive macaque CD4+ and CD8+ T cells in vivo. J. Virol. *78*, 9740–9749.

23. Nugeyre, M.T., Monceaux, V., Beq, S., Cumont, M.C., Ho Tsong Fang, R., Chêne, L., Morre, M., Barré-Sinoussi, F., Hurtrel, B., and Israël, N. (2003). IL-7 stimulates T cell renewal without increasing viral replication in simian immunodeficiency virus-infected macaques. J. Immunol. *171*, 4447–4453. https://doi.org/10.4049/jimmunol.171.8.4447.

24. Okoye, A.A., Rohankhedkar, M., Konfe, A.L., Abana, C.O., Reyes, M.D., Clock, J.A., Duell, D.M., Sylwester, A.W., Sammader, P., Legasse, A.W., et al. (2015). Effect of IL-7 therapy on naive and memory T cell homeostasis in aged rhesus macaques. J. Immunol. *195*, 4292–4305. https://doi.org/10.4049/jimmunol.1500609.

25. Vassena, L., Miao, H., Cimbro, R., Malnati, M.S., Cassina, G., Proschan, M.A., Hirsch, V.M., Lafont, B.A., Morre, M., Fauci, A.S., and Lusso, P. (2012). Treatment with IL-7 prevents the decline of circulating CD4+ T cells during the acute phase of SIV infection in rhesus macaques. PLoS Pathog. *8*, e1002636. https://doi.org/10.1371/journal.ppat.1002636.

26. Bergamaschi, C., Watson, D.C., Valentin, A., Bear, J., Peer, C.J., Figg, W.D., Felber, B.K., Pavlakis, G.N., and Pavlakis, G.N. (2018). Optimized administration of hetIL-15 expands lymphocytes and minimizes toxicity in rhesus macaques. Cytokine *108*, 213–224. https://doi.org/10.1016/j.cyto.2018.01.011.

27. Watson, D.C., Moysi, E., Valentin, A., Bergamaschi, C., Devasundaram, S., Fortis, S.P., Bear, J., Chertova, E., Bess, J., Jr., Sowder, R., et al. (2018). Treatment with native heterodimeric IL-15 increases cytotoxic lymphocytes and reduces SHIV RNA in lymph nodes. PLoS Pathog. *14*, e1006902. https://doi.org/10.1371/journal.ppat.1006902.

28. Vogelzang, A., McGuire, H.M., Yu, D., Sprent, J., Mackay, C.R., and King, C. (2008). A fundamental role for interleukin-21 in the generation of T follicular helper cells. Immunity *29*, 127–137. https://doi.org/10.1016/j.immuni.2008.06.001.

29. Asselin-Paturel, C., and Trinchieri, G. (2005). Production of type I interferons: plasmacytoid dendritic cells and beyond. J. Exp. Med. *202*, 461–465. https://doi.org/10.1084/jem.20051395.

30. Zhang, H., Gregorio, J.D., Iwahori, T., Zhang, X., Choi, O., Tolentino, L.L., Prestwood, T., Carmi, Y., and Engleman, E.G. (2017). A distinct subset of plasmacytoid dendritic cells induces activation and differentiation of B and T lymphocytes. Proc. Natl. Acad. Sci. USA *114*, 1988–1993. https://doi.org/10.1073/pnas.1610630114.

31. Sieling, P.A., Sakimura, L., Uyemura, K., Yamamura, M., Oliveros, J., Nickoloff, B.J., Rea, T.H., and Modlin, R.L. (1995). IL-7 in the cell-mediated immune response to a human pathogen. J. Immunol. *154*, 2775–2783.

32. Futagami, S., Hiratsuka, T., Suzuki, K., Kusunoki, M., Wada, K., Miyake, K., Ohashi, K., Shimizu, M., Takahashi, H., Gudis, K., et al. (2006). Gammadelta T cells increase with gastric mucosal interleukin (IL)-7, IL-1beta, and Helicobacter pylori urease specific immunoglobulin levels via CCR2

upregulation in Helicobacter pylori gastritis. J. Gastroenterol. Hepatol. *21*, 32–40. https://doi.org/10.1111/j.1440-1746.2005.04148.x.

33. Sawa, Y., Arima, Y., Ogura, H., Kitabayashi, C., Jiang, J.J., Fukushima, T., Kamimura, D., Hirano, T., and Murakami, M. (2009). Hepatic interleukin-7 expression regulates T cell responses. Immunity *30*, 447–457. https://doi.org/10.1016/j.immuni.2009.01.007.

34. Wallington, J.C., Williams, A.P., Staples, K.J., and Wilkinson, T.M.A. (2018). IL-12 and IL-7 synergize to control mucosal-associated invariant T-cell cytotoxic responses to bacterial infection. J. Allergy Clin. Immunol. *141*, 2182–2195.e6. https://doi.org/10.1016/j.jaci.2017.08.009.

35. Sheikh, A., Jackson, J., Shim, H.B., Yau, C., Seo, J.H., and Abraham, N. (2022). Selective dependence on IL-7 for antigen-specific CD8 T cell responses during airway influenza infection. Sci. Rep. *12*, 135. https://doi.org/10.1038/s41598-021-03936-y.

36. Beq, S., Rozlan, S., Gautier, D., Parker, R., Mersseman, V., Schilte, C., Assouline, B., Rancé, I., Lavedan, P., Morre, M., and Cheynier, R. (2009). Injection of glycosylated recombinant simian IL-7 provokes rapid and massive T-cell homing in rhesus macaques. Blood *114*, 816–825. https://doi.org/10.1182/blood-2008-11-191288.

37. Ponte, R., Rancez, M., Figueiredo-Morgado, S., Dutrieux, J., Fabre-Mersseman, V., Charmeteau-de-Muylder, B., Guilbert, T., Routy, J.P., Cheynier, R., and Couëdel-Courteille, A. (2017). Acute simian immunodeficiency virus infection triggers early and transient interleukin-7 production in the gut, leading to enhanced local chemokine expression and intestinal immune cell homing. Front. Immunol. *8*, 588. https://doi.org/10.3389/fimmu.2017.00588.

38. Luther, S.A., Ansel, K.M., and Cyster, J.G. (2003). Overlapping roles of CXCL13, interleukin 7 receptor alpha, and CCR7 ligands in lymph node development. J. Exp. Med. *197*, 1191–1198. https://doi.org/10.1084/jem.20021294.

39. Onder, L., and Ludewig, B. (2018). A fresh view on lymph node organogenesis. Trends Immunol. *39*, 775–787. https://doi.org/10.1016/j.it.2018.08.003.

40. Onder, L., Mörbe, U., Pikor, N., Novkovic, M., Cheng, H.W., Hehlgans, T., Pfeffer, K., Becher, B., Waisman, A., Rülicke, T., et al. (2017). Lymphatic endothelial cells control initiation of lymph node organogenesis. Immunity *47*, 80–92.e4. https://doi.org/10.1016/j.immuni.2017.05.008.

41. Onder, L., Narang, P., Scandella, E., Chai, Q., Iolyeva, M., Hoorweg, K., Halin, C., Richie, E., Kaye, P., Westermann, J., et al. (2012). IL-7-producing stromal cells are critical for lymph node remodeling. Blood *120*, 4675–4683. https://doi.org/10.1182/blood-2012-03-416859.

42. Roozendaal, R., and Mebius, R.E. (2011). Stromal cell-immune cell interactions. Annu. Rev. Immunol. *29*, 23–43. https://doi.org/10.1146/annurev-immunol-031210-101357.

43. Chappaz, S., and Finke, D. (2010). The IL-7 signaling pathway regulates lymph node development independent of peripheral lymphocytes. J. Immunol. *184*, 3562–3569. https://doi.org/10.4049/jimmunol.0901647.

44. Mebius, R.E. (2003). Organogenesis of lymphoid tissues. Nat. Rev. Immunol. *3*, 292–303. https://doi.org/10.1038/nri1054.

45. Schmutz, S., Bosco, N., Chappaz, S., Boyman, O., Acha-Orbea, H., Ceredig, R., Rolink, A.G., and Finke, D. (2009). Cutting edge: IL-7 regulates the peripheral pool of adult ROR gamma+ lymphoid tissue inducer cells. J. Immunol. *183*, 2217–2221. https://doi.org/10.4049/jimmunol.0802911.

46. Meier, D., Bornmann, C., Chappaz, S., Schmutz, S., Otten, L.A., Ceredig, R., Acha-Orbea, H., and Finke, D. (2007). Ectopic lymphoid-organ development occurs through interleukin 7-mediated enhanced survival of lymphoid-tissue-inducer cells. Immunity *26*, 643–654. https://doi.org/10.1016/j.immuni.2007.04.009.

47. Havenar-Daughton, C., Lindqvist, M., Heit, A., Wu, J.E., Reiss, S.M., Kendric, K., Bélanger, S., Kasturi, S.P., Landais, E., Akondy, R.S., et al. (2016). CXCL13 is a plasma biomarker of germinal center activity. Proc. Natl. Acad. Sci. USA *113*, 2702–2707. https://doi.org/10.1073/pnas.1520112113.

48. Crotty, S. (2011). Follicular helper CD4 T cells (TFH). Annu. Rev. Immunol. *29*, 621–663. https://doi.org/10.1146/annurev-immunol-031210-101400.

49. Crotty, S. (2019). T follicular helper cell biology: a decade of Discovery and diseases. Immunity *50*, 1132–1148. https://doi.org/10.1016/j.immuni.2019.04.011.

50. Gong, F., Zheng, T., and Zhou, P. (2019). T follicular helper cell subsets and the associated cytokine IL-21 in the pathogenesis and therapy of asthma. Front. Immunol. *10*, 2918. https://doi.org/10.3389/fimmu.2019.02918.

51. Ozaki, K., Spolski, R., Feng, C.G., Qi, C.F., Cheng, J., Sher, A., Morse, H.C., 3rd, Liu, C., Schwartzberg, P.L., and Leonard, W.J. (2002). A critical role for IL-21 in regulating immunoglobulin production. Science *298*, 1630–1634. https://doi.org/10.1126/science.1077002.

52. Spolski, R., and Leonard, W.J. (2014). Interleukin-21: a double-edged sword with therapeutic potential. Nat. Rev. Drug Discov. *13*, 379–395. https://doi.org/10.1038/nrd4296.

53. Li, Y., Zhou, M., Luo, Z., Zhang, Y., Cui, M., Chen, H., et al. (2017). Overexpression of interleukin-7 extends the humoral immune response induced by rabies vaccination. J. Virol. *91*. e02324–16. https://doi.org/10.1128/jvi.02324-16.

54. Seo, Y.B., Im, S.J., Namkoong, H., Kim, S.W., Choi, Y.W., Kang, M.C., Lim, H.S., Jin, H.T., Yang, S.H., Cho, M.L., et al. (2014). Crucial roles of interleukin-7 in the development of T follicular helper cells and in the induction of humoral immunity. J. Virol. *88*, 8998–9009. https://doi.org/10.1128/jvi.00534-14.

55. Logerot, S., Figueiredo-Morgado, S., Charmeteau-de-Muylder, B., Sandouk, A., Drillet-Dangeard, A.S., Bomsel, M., Bourgault-Villada, I., Couëdel-Courteille, A., Cheynier, R., and Rancez, M. (2021). IL-7-Adjuvanted vaginal vaccine elicits strong mucosal immune responses in non-human primates. Front. Immunol. *12*, 614115. https://doi.org/10.3389/fimmu.2021.614115.

56. Zhang, Y., Liang, S., Li, X., Wang, L., Zhang, J., Xu, J., Huo, S., Cao, X., Zhong, Z., and Zhong, F. (2015). Mutual enhancement of IL-2 and IL-7 on DNA vaccine immunogenicity mainly involves regulations on their receptor expression and receptor-expressing lymphocyte generation. Vaccine *33*, 3480–3487. https://doi.org/10.1016/j.vaccine.2015.05.068.

57. Pham, T.N.Q., Meziane, O., Miah, M.A., Volodina, O., Colas, C., Béland, K., Li, Y., Dallaire, F., Keler, T., Guimond, J.V., et al. (2019). Flt3L-Mediated expansion of plasmacytoid dendritic cells suppresses HIV infection in humanized mice. Cell Rep. *29*, 2770–2782.e5. https://doi.org/10.1016/j.celrep.2019.10.094.

58. Pulendran, B., Banchereau, J., Burkeholder, S., Kraus, E., Guinet, E., Chalouni, C., Caron, D., Maliszewski, C., Davoust, J., Fay, J., and Palucka, K. (2000). Flt3-ligand and granulocyte colony-stimulating factor mobilize distinct human dendritic cell subsets in vivo. J. Immunol. *165*, 566–572. https://doi.org/10.4049/jimmunol.165.1.566.

59. Anandasabapathy, N., Breton, G., Hurley, A., Caskey, M., Trumpfheller, C., Sarma, P., Pring, J., Pack, M., Buckley, N., Matei, I., et al. (2015). Efficacy and safety of CDX-301, recombinant human Flt3L, at expanding dendritic cells and hematopoietic stem cells in healthy human volunteers. Bone Marrow Transplant. *50*, 924–930. https://doi.org/10.1038/bmt.2015.74.

60. Vogt, T.K., Link, A., Perrin, J., Finke, D., and Luther, S.A. (2009). Novel function for interleukin-7 in dendritic cell development. Blood *113*, 3961–3968. https://doi.org/10.1182/blood-2008-08-176321.

61. Honda, K., Yanai, H., Negishi, H., Asagiri, M., Sato, M., Mizutani, T., Shimada, N., Ohba, Y., Takaoka, A., Yoshida, N., and Taniguchi, T. (2005). IRF-7 is the master regulator of type-I interferon-dependent immune responses. Nature *434*, 772–777. https://doi.org/10.1038/nature03464.

62. Jefferies, C.A. (2019). Regulating IRFs in IFN driven disease. Front. Immunol. *10*, 325. https://doi.org/10.3389/fimmu.2019.00325.

63. Kang, M.C., Park, H.W., Choi, D.H., Choi, Y.W., Park, Y., Sung, Y.C., and Lee, S.W. (2017). Plasmacytoid dendritic cells contribute to the protective immunity induced by intranasal treatment with fc-fused interleukin-7 against lethal influenza virus infection. Immune Netw. *17*, 343–351. https://doi.org/10.4110/in.2017.17.5.343.

64. Hadjadj, J., Yatim, N., Barnabei, L., Corneau, A., Boussier, J., Smith, N., Péré, H., Charbit, B., Bondet, V., Chenevier-Gobeaux, C., et al. (2020). Impaired type I interferon activity and inflammatory responses in severe COVID-19 patients. Science *369*, 718–724. https://doi.org/10.1126/science.abc6027.

65. Sa Ribero, M., Jouvenet, N., Dreux, M., and Nisole, S. (2020). Interplay between SARS-CoV-2 and the type I interferon response. PLoS Pathog. *16*, e1008737. https://doi.org/10.1371/journal.ppat.1008737.

66. Tan, L., Wang, Q., Zhang, D., Ding, J., Huang, Q., Tang, Y.Q., Wang, Q., and Miao, H. (2020). Lymphopenia predicts disease severity of COVID-19: a descriptive and predictive study. Signal Transduct. Target.Ther. *5*, 33. https://doi.org/10.1038/s41392-020-0148-4.

67. Tavakolpour, S., Rakhshandehroo, T., Wei, E.X., and Rashidian, M. (2020). Lymphopenia during the COVID-19 infection: what it shows and what can be learned. Immunol.Lett. *225*, 31–32. https://doi.org/10.1016/j.imlet.2020.06.013.

68. Toor, S.M., Saleh, R., Sasidharan Nair, V., Taha, R.Z., and Elkord, E. (2021). T-cell responses and therapies against SARS-CoV-2 infection. Immunology *162*, 30–43. https://doi.org/10.1111/imm.13262.

69. Deleage, C., Schuetz, A., Alvord, W.G., Johnston, L., Hao, X.P., Morcock, D.R., Rerknimitr, R., Fletcher, J.L.K., Puttamaswin, S., Phanuphak, N., et al. (2016). Impact of early cART in the gut during acute HIV infection. JCI Insight *1*, e87065. https://doi.org/10.1172/jci.insight.87065.

STAR★METHODS

KEY RESOURCES TABLE

REAGENT or RESOURCE	SOURCE	IDENTIFIER
Antibodies		
FITC Mouse Anti-Human CD95 Clone DX2 (RUO)	BD Biosciences	Cat#556640; RRID: AB_396506
BV650 Mouse Anti-Ki-67 Clone B56 (RUO)	BD Biosciences	Cat#563757; RRID: AB_2688008
ROR gamma (t) Monoclonal Antibody (AFKJS-9), APC	eBioscience	Cat#17-6988; RRID: AB_10609207
Mouse antiHuman CD45RA:Alexa Fluor® 700	AbD serotec	Cat#MCA88A700; RRID: AB_844506
Brilliant Violet 421™ anti-human XCR1 Antibody Clone S15046E	Biolegend	Cat#372610; RRID: AB_2687373
PE-CF594 Mouse Anti-Human CD32 Clone FLI8.26 (also known as 8.26) (RUO)	BD Biosciences	Cat#565647; RRID: AB_2739323
Brilliant Violet 711™ anti-human CD1c Antibody Clone L161	Biolegend	Cat#331536; RRID: AB_2629760
PE/Cyanine7 anti-human CD183 (CXCR3) Antibody Clone G025H7	Biolegend	Cat#353720; RRID: AB_11219383
Granzyme B Monoclonal Antibody (GB12), PE	eBiosciences	Cat#MHGB04; RRID: AB_10372671
BV650 Mouse Anti-Human CD141 Clone 1A4 (RUO)	BD Biosciences	Cat#740604; RRID: AB_2740304
BV480 Mouse Anti-Human CD16 Clone 3G8 (RUO)	BD Biosciences	Cat#566108; RRID: AB_2739510
BV605 Mouse Anti-Human CD134 Clone L106 (RUO)	BD Biosciences	Cat#745217; RRID: AB_2742808
Brilliant Violet 785™ anti-human CD28 Antibody Clone CD28.2	Biolegend	Cat#302950; RRID: AB_2632607
BV650 Mouse Anti-Human CD196 (CCR6) Clone 11A9 (RUO)	BD Biosciences	Cat#563922; RRID: AB_2738488
BV605 Rat Anti-Human CCR7 (CD197) Clone 3D12 (RUO)	BD Biosciences	Cat#563711; RRID: AB_2738385
BV605 Mouse Anti-Human CD27 Clone M-T271 (RUO)	BD Biosciences	Cat#740398; RRID: AB_2740128
BV786 Mouse Anti-Human CD123 Clone 7G3 (RUO)	BD Biosciences	Cat#564196; RRID: AB_2738662
BUV395 Mouse Anti-Human CD4 Clone L200 (RUO)	BD Biosciences	Cat#564107; RRID: AB_2738596
BUV563 Mouse Anti-Human CD3 Clone SP34-2 (RUO)	BD Biosciences	Cat#741412; RRID: AB_2870901
BUV496 Mouse Anti-Human CD8 Clone RPA-T8	BD Biosciences	Cat#612943; RRID: AB_2916884
BUV661 Mouse Anti-Human HLA-DR Clone G46-6 (RUO)	BD Biosciences	Cat#612981; RRID: AB_2870252
BUV737 Mouse Anti-Human CD69 Clone FN50 (also known as FN 50) (RUO)	BD Biosciences	Cat#612818; RRID: AB_2870142
BUV737 Mouse Anti-Human CD25 Clone M-A251 (RUO)	BD Biosciences	Cat#741832; RRID: AB_2871167

(*Continued on next page*)

Continued

REAGENT or RESOURCE	SOURCE	IDENTIFIER
PE-CF594 Mouse Anti-Human CD20 Clone 2H7 (RUO)	BD Biosciences	Cat#562550; RRID: AB_2737646
BUV805 Mouse Anti-Human CD14 Clone M5E2 (RUO)	BD Biosciences	Cat#565779; RRID: AB_2716868
PE-CF594 Mouse Anti-Human Bcl-2 Clone Bcl-2/100 (RUO)	BD Biosciences	Cat#563601; RRID: AB_2738307
PE/Cyanine5 anti-human CD154 Antibody Clone 24-31	Biolegend	Cat#310806; RRID: AB_314829
PE/Cyanine5 anti-human CD127 (IL-7Rα) Antibody Clone A019D5	Biolegend	Cat#351324; RRID: AB_10915554
APC/Cyanine7 anti-human CD279 (PD-1) Antibody Clone EH12.2H7	Biolegend	Cat#329922; RRID: AB_10933429
CD20 for IHC	Dako	Agilent Cat#M0755; RRID: AB_2282030
BCL6 for IHC	Dako	Agilent Cat# M7211, RRID: AB_2063451
CD4 for IFA	R&D Systems	Cat#AF-379-NA; RRID: AB_354469
Ki67 for IFA	Thermo Fisher Scientific	Cat#MA5-14520; RRID: AB_10979488
donkey anti-goat IgG-Alexa 488, donkey anti-mouse IgG-Alexa 594 and donkey anti-rabbit Alexa 647	Molecular Probes and Thermo Fisher Scientific	Cat# A-11055 Cat# A-21203 Cat# A-32795
RPMI1640	Gibco	Cat#11875-093
Biological samples		
Plasma	this study	N/A
Peripheral blood mononuclear cells (PBMC)	this study	N/A
Lymph node mononuclear cells (LNMC)	this study and controls	N/A
Splenocytes	this study and controls	N/A
human serum	Sigma	Cat#H4522
RLT Buffer	Qiagen	Cat#101576
Chemicals, peptides, and recombinant proteins		
Ficoll-hypaque	GE Healthcare	Cat#17-1440-03
FoxP3 washing buffer	eBioscience	Cat#00-5523-00
Rhesus macaque IL-7	In house	N/A
R848	Invivogen	Cat#tlrl-r848
ODN	Invivogen	Cat#tlrl-2216
Mouse Polink 1 horseradish peroxidase	Golden Bridge International	Cat#D24-110
Permount	Fisher Scientific	Cat#SP15-100
ImmPACT DAB	Vector Laboratories	Cat#SK-4105
Critical commercial assays		
IL-7 ELISA	R&D Systems	Cat#DY207
IL-21 ELISA	Biolegend	Cat#433804
CXCL13 ELISA	Invitrogen	Cat#EMCXCL13
IFN-a ELISA	PBL Assay Science	Cat#46100-1
nCounter NHP Immunology Panel	Nanostring Technology	Cat#XT-CSO-NHPIM1-12
NHP U-plex Biomarker 61-plex	Meso Scale Diagnostics, LLC	Cat#K15082K
RNeasy kit	Qiagen	Cat#74104

(*Continued on next page*)

Continued

REAGENT or RESOURCE	SOURCE	IDENTIFIER
Deposited data		
Cytokine expression data, transcriptomics data from nanostring and analysis code	This paper	https://github.com/NCI-VB/pandit_IL7
Experimental models: Cell lines		
HEK293H	Invitrogen	Cat#11631017
Experimental models: Organisms/strains		
M. mulatta-Indian Rhesus macaques	Bioqual	N/A
Software and algorithms		
GraphPad Prism version 9.0.2 for MacOS	GraphPad Software	N/A
FlowJo Software v10	BD	N/A
SoftMax Pro	Molecular Devices, LLC	N/A
NIH Integrated Data Analysis Platform	This paper	https://nidap.nih.gov/workspace
FIJI software	Open Source software ImageJ	N/A
Other		
Fortessa and Symphony Flow Cytometers	BD Biosciences	N/A
Bio-Plex Instrument	Meso Scale Diagnostics, LLC	N/A
SpectraMax Plus 384 Microplate Spectrophotometer	Molecular Devices, LLC	N/A
ScanScope AT2 System	Aperio Technologies	N/A
Zeiss Axio Imager Z1 microscope	Zeiss	N/A
Hollow Fiber System	FiberCell System Inc	N/A
Tangential Flow filtration	TangenX	N/A
Capto Q resin	GE Healthcare Science	N/A
Dionex HPLC system	Thermo Fisher	N/A

RESOURCE AVAILABILITY

Lead contact

Further information and requests for resources and reagents should be directed to and will be fulfilled by the lead contact, (George.pavlakis@nih.gov).

Materials availability

This study generated glycosylated macaque IL-7 produced in human cells.

Data and code availability

- Data and analysis generated during the study are available at https://github.com/NCI-VB/pandit_IL7. Analysis was performed on Palantir platform and deposited on NIDAP.
- This paper does not report original code.
- Any additional information required to reanalyze the data reported in this paper is available from the lead contactupon request.

EXPERIMENTAL MODEL AND SUBJECTDETAILS

The macaque studies were conducted in compliance with all applicable state and federal regulations and were approved by BIOQUAL's Institutional Animal Care and Use Committee (IACUC). A total of ten adult rhesus macaques of Indian origin were used in this study.

METHOD DETAILS

Purification of mammalian cell produced rhesus macaque IL-7

A plasmid (AG292) optimized for the efficient expression of rhesus macaque IL-7 was used for the generation of stable clonal cell lines. HEK293H cells (Invitrogen) were stably transfected with linearized plasmid encoding macaque IL-7 DNA by the calcium phosphate coprecipitation technique. The highest IL-7 producer clone was used for cytokine production using serum-free media in a hollow fiber system (FiberCell Systems Inc). Glucose consumption was measured daily, and media was replaced when the glucose concentration dropped below 100 mg/dL. Cell supernatants (20 mL) were harvested daily for up to 2 months and assayed for IL-7 levels by ELISA (R&D Systems, human IL-7 ELISA, cat#DY207). To purify HEK293-produced recombinant IL-7, crude supernatants were subjected to a three-step purification: (i) concentration, using tandem tangential flow filtration (TangenX); (ii) anion exchange chromatography using Capto Q resin (GE Healthcare Science), and (iii) second purification of pooled IL-7 containing fractions by RP-HPLC using a Dionex HPLC system (Figure S1). The resulting glycosylated macaque IL-7 was pure of contaminants and stable.

IL-7 treatment

Male adult macaques (n = 6) with a mean weight of 7.6 kg (range: 5.2–12.2 kg) were treated with a step-dose regimen. The animals received three subcutaneous injections with increased doses of rhesus macaque rmIL-7 (50, 100 and 200 μg/kg) during an 8-day treatment cycle (day 1, 4 and 8). Male adult macaques (n = 4) with a mean weight of 7.5 kg (range 7.4–7.7 kg) received 3 doses of rhesus macaque rmIL-7 (100 or 200 μg/kg; 2 animals each) during an 8-day treatment cycle (day 1, 4 and 8). Peripheral blood samples were collected immediately before and 4, 24 and 48 h after each injection. Only the animals from the step-dose were sacrificed two days after the last injection, and blood and several lymphoid tissues, including axillary, inguinal, mediastinal, mesenteric LN and spleen were collected.

Isolation of PBMCs and preparation of single cell suspensions from LNs and spleen

PBMCs were isolated using Ficoll-hypaque (GE Healthcare) based on the manufacturer's instructions. Lymph nodes and spleens were transported on wet ice in complete RPMI medium within 2 h from surgery. To isolate mononuclear cells, lymph nodes and spleen tissues were crushed on a 100 mm strainer (BD) using the plunger of a 3 mL sterile syringe. Cells were washed in PBS, counted, and cryopreserved or directly stained for flow cytometric analysis.

Immune phenotyping and flow cytometry

Mononuclear cells were washed with PBS supplemented with 0.2% heat-inactivated human serum (Sigma) and incubated with different cocktails of a panel of fluorophore-labelled monoclonal antibodies for 20 min at room temperature as listed in STAR Methods. After cell surface staining, the cells were washed once and fixed/permeabilized using the FoxP3 staining kit (eBioscience cat# 00-5523-00). After 30 min incubation at 4°C, the cells were washed with FoxP3 washing buffer and intracellularly stained with cocktails of fluorophore-labelled monoclonal antibodies targeting intracellular antigens Mouse Anti-Ki-67; anti-ROR gammaT; anti-Granzyme B for 20 min. The cells were washed and resuspended in PBS for flow cytometry analysis. The samples were acquired in a Symphony or Fortessa flow cytometers (BD Biosciences, San Jose, CA), and the data were analyzed using the FlowJo software platform (Tree Star, Inc., Ashland, OR).

Measurement of plasma cytokines

CXCL-13 (Invitrogen cat# EMCXCL13), IL-7 (R&D Systems cat#DY207) and IL-21 (Biolegend cat#433804) were measured in plasma by commercial ELISA according to the manufacturer's instructions. A panel of cytokines, chemokines and growth factors was measured using a chemiluminescent multiplex assay (U-PLEX Biomarker Group 1 NHP 61-Plex) from Meso Scale Diagnostics LLC.

Gene expression analysis by nCounter NHP Immunology Panel

Cells were lysed using RLT buffer and stored at −80°C. RNA was extracted using RNeasy kit (QIAGEN) according to the manufacturer's instructions with on-column DNase digestion. nCounter NHP Immunology Panel (NanoString Technologies cat#XT-CSO-NHPIM1-12) was used to monitor the expression of a panel of 776 genes. The RNA was run on the nCounter Analysis System (NanoString Technologies) at the

Laboratory of Molecular Technology (Advance Technology Program, Frederick National Laboratory). Total RNA was loaded at 100 ng per sample. Hybridizations were performed for 17–22 h, and the counts were gathered by scanning on HIGH mode for 280 fields of view per sample. Analysis was performed in collaboration with CCR Collaborative Bioinformatics Resource using the Palantir platform (Palantir Technologies). To normalize data, voom transformation and quantile normalization were applied. To define differentially expressed genes, log2 fold change and $p < 0.05$ (adjusted for multiple comparison, p value) difference between groups (Tables S2 and S3) was used. Enriched pathways were identified using the GO signature database, using a cut-off $p < 0.05$. Heatmaps were represented as Z-score centered and rescaled.

Immunohistochemistry for B cells and germinal center count

Immunohistochemical staining and quantitative image analysis were performed as previously described.[69] In brief, immunohistochemistry was performed using a biotin-free polymer approach (Golden Bridge International) on 5-μm tissue sections mounted on glass slides, dewaxed and rehydrated with double-distilled water. Heat-induced epitope retrieval was performed by heating sections in 0.01% citraconic anhydride containing 0.05% Tween 20 for CD20 and BCL6 antibodies. Slides were incubated for 1 h at room temperature with mouse anti-CD20 (DAKO, clone L26, dilution 1:500, cat# M075501-2) or mouse anti-BCL6 (DAKO, clone PG-B6p, dilution 1:100, cat# GA62561-2) diluted in blocking buffer. After washing in 1× TBS with 0.05% Tween 20, endogenous peroxidases were blocked using 1.5% (v/v) H_2O_2 in TBS, pH 7.4, for 5 min, and the slides were incubated with mouse Polink 1 (Golden Bridge International) horseradish peroxidase and developed with ImmPACT DAB (3,3′-diaminobenzidine; Vector Laboratories), according to the manufacturer's recommendations. All slides were washed in tap water, counterstained with hematoxylin, mounted in Permount (Fisher Scientific), and scanned at high magnification (×200) using the ScanScope AT2 System (Aperio Technologies), yielding high-resolution data from the entire tissue section. BCF and GC were manually counted from these whole-tissue scans.

Immuno-histofluorescence for Tfh Ki67$^+$ quantification

IFA was performed by combining ON goat anti-CD4 (R&D system, 1:1000 cat#AF-379-NA), rabbit anti-KI67 (Thermo science, 1:200 cat# MA5-14520) and mouse anti-BCL6 (DAKO, 1:100) in TBS-tween. Slides were washed, incubated with secondary antibodies donkey anti-goat IgG-Alexa 488, donkey anti-mouse IgG-Alexa 594 and donkey anti-rabbit Alexa 647 (Molecular Probes and ThermoFisher Scientific) for 1hat room temperature. To decrease autofluorescence, the tissues were incubated with Sudan Black solution (0.1% in 80% ethanol [ENG Scientific, Inc.] + 1x TBS); for 30 min at room temperature, washed, counterstained with DAPI (RTU; ACD) for 10 min, washed in TBS and cover slipped using Prolong Gold reagent (Invitrogen). IFA images were visualized and photographed with Zeiss Axio Imager Z1 microscope (Zeiss) affixed with Apotome and total Tfh and Tfh expressing Ki67 were counted using FIJI software.

Ex vivo stimulation of lymph node mononuclear cells (LNMC) with TLR ligands

Mononuclear cells were obtained from LN collected before and after *in vivo* IL-7 treatment. The cells were seeded in RPMI complete medium at a cell density of 2×10^6/mL and treated with the TLR agonists R848 (Invivogen cat# tlrl-r848) or ODN (Invivogen cat# tlrl-2216) at a final concentration of 2 mM. After 24 h incubation, culture supernatants were collected and the concentration of IFN-α2a was measured by ELISA (PBL Assay Science cat#46100-1) per manufacturer's instructions.

Statistics

Data were plotted as median. Differences between before and after IL-7 treatment were evaluated by a paired T-test for pre and post comparisons and unpaired T-test for comparisons with control and treated animals. pvalues < 0.05 were considered statistically significant. Prism 9.2.0 software package was used for analysis. The statistical tools, methods, and threshold for each analysis are described in the STAR Methods section, the Result section or detailed in the figure legends.

Bioinformatics

Biomarker analysis was performed with a workflow written in R and through a user interface developed on the Foundry Platform (Palantir Technologies). The limma package was used to compare biomarker changes between time points, setting significance for False Discovery Rate (FDR) < 0.05.

QUANTIFICATION AND STATISTICAL ANALYSIS

Software

All software is freely or commercially available and is listed in the STAR Methods description and key resources table.